Resource

Molecular Cell

Live-Cell Single RNA Imaging Reveals Bursts of Translational Frameshifting

Graphical Abstract

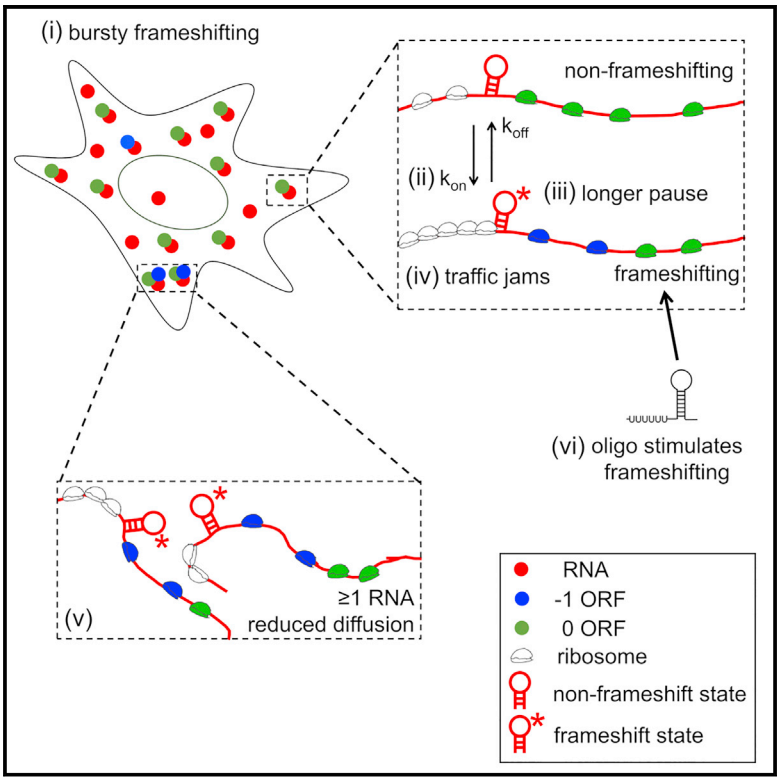

Highlights

- A multi-frame tag can monitor single-RNA translation in two open reading frames
- A bursty model captures frameshift kinetics for the HIV-1 frameshift sequence (FSS)
- Frameshifting persists on a subset of RNA and can be stimulated by an RNA oligo
- Frameshifted ribosomes take longer to clear the FSS and cause ribosome traffic jams

Authors

Kenneth Lyon, Luis U. Aguilera, Tatsuya Morisaki, Brian Munsky, Timothy J. Stasevich

Correspondence

brian.munsky@colostate.edu (B.M.), tim.stasevich@colostate.edu (T.J.S.)

In Brief

A multi-frame tag and stochastic model visualize and quantify bursty frameshifting of single RNA encoding the HIV-1 frameshift sequence (FSS). Frameshifting involves elongation pauses that induce ribosomal traffic jams. Frameshifting occurs in slowly diffusing RNA clusters and can be stimulated by an RNA oligo encoding the FSS.

Lyon et al., 2019, Molecular Cell *75*, 1–12
July 11, 2019
https://doi.org/10.1016/j.molcel.2019.05.002

CellPress

Please cite this article in press as: Lyon et al., Live-Cell Single RNA Imaging Reveals Bursts of Translational Frameshifting, Molecular Cell (2019), https://doi.org/10.1016/j.molcel.2019.05.002

Molecular Cell
Resource

Live-Cell Single RNA Imaging Reveals Bursts of Translational Frameshifting

Kenneth Lyon,[1] Luis U. Aguilera,[2] Tatsuya Morisaki,[1] Brian Munsky,[2,*] and Timothy J. Stasevich[1,3,4,*]
[1]Department of Biochemistry and Molecular Biology, Institute of Genome Architecture and Function, Colorado State University, Fort Collins, CO 80523, USA
[2]Department of Chemical and Biological Engineering and School of Biomedical Engineering, Colorado State University, Fort Collins, CO 80523, USA
[3]World Research Hub Initiative, Institute of Innovative Research, Tokyo Institute of Technology, Yokohama, Kanagawa 226-8503, Japan
[4]Lead Contact
*Correspondence: brian.munsky@colostate.edu (B.M.), tim.stasevich@colostate.edu (T.J.S.)
https://doi.org/10.1016/j.molcel.2019.05.002

SUMMARY

Ribosomal frameshifting during the translation of RNA is implicated in human disease and viral infection. While previous work has uncovered many details about single RNA frameshifting kinetics *in vitro*, little is known about how single RNA frameshift in living systems. To confront this problem, we have developed technology to quantify live-cell single RNA translation dynamics in frameshifted open reading frames. Applying this technology to RNA encoding the HIV-1 frameshift sequence reveals a small subset (~8%) of the translating pool robustly frameshift. Frameshifting RNA are translated at similar rates as non-frameshifting RNA (~3 aa/s) and can continuously frameshift for more than four rounds of translation. Fits to a bursty model of frameshifting constrain frameshifting kinetic rates and demonstrate how ribosomal traffic jams contribute to the persistence of the frameshifting state. These data provide insight into retroviral frameshifting and could lead to alternative strategies to perturb the process in living cells.

INTRODUCTION

Frameshifting is a fundamental biological process in which a ribosome translating an RNA slips by ±1 nt, resulting in the translation of an entirely different peptide sequence from that point forward. While frameshifting is generally detrimental to protein fidelity (Belew et al., 2014; Choi et al., 2015), the process effectively creates two distinct proteins from a single RNA (Clark et al., 2007; Meydan et al., 2017; Yordanova et al., 2015). Viruses exploit this aspect of frameshifting to minimize their genomes and to successfully replicate in host cells (Atkins et al., 2016; Brierley and Dos Ramos, 2006; Brierley et al., 1989; Caliskan et al., 2015; Cardno et al., 2015; Mouzakis et al., 2013). A prototypical example is HIV, which utilizes frameshifting to translate the Gag-Pol proteins from a single viral RNA (Guerrero et al., 2015).

Although frameshifting has been extensively studied *in vitro* and in bulk assays (Caliskan et al., 2014; Charbonneau et al., 2012; Chen et al., 2014; Lopinski et al., 2000; Mouzakis et al., 2013; Ritchie et al., 2017), the process has never been observed at the single-molecule level in living cells. This leaves many basic questions about frameshifting unresolved. In particular, it is not clear how heterogeneous frameshifting is from one RNA to another, nor is it clear if single RNA continuously frameshift in a constitutive fashion or if instead they frameshift in prolonged bursts, as has been observed for transcription (Lionnet and Singer, 2012) and canonical translation (Wu et al., 2016). Finally, the localization of frameshifting has never been investigated, so it is not clear if frameshifting occurs all throughout the cell or is instead preferentially localized to specific sub-cellular regions. In the case of HIV-1 Gag-Pol, for example, previous assays have shown that 5% to 10% of translated protein product is frameshifted (Brierley and Dos Ramos, 2006; Dulude et al., 2002; Grentzmann et al., 1998; Mouzakis et al., 2013). This is thought to occur when ribosomes translate through a specialized frameshift sequence (FSS) containing a stem loop structure that slows down incoming ribosomes and causes them to slip back one nucleotide on a slippery sequence preceding the stem loop. Whether or not this occurs constitutively and with equal probability on all HIV-1 RNA or if instead it occurs on a specialized subset that are in the right place, at the right time, and with the right factors remains to be determined.

To directly address these sorts of questions, we have developed technology to visualize and quantify single-RNA frameshifting dynamics in living cells. Using multi-frame repeat epitopes, complementary high-affinity fluorescent probes that selectively bind the epitopes, and multicolor single-molecule microscopy, we are able to simultaneously monitor the translation of single RNA into two unique nascent polypeptide chains encoded in shifted open reading frames. Application to the HIV-1 FSS uncovers unexpected heterogeneity in the production of frameshifted product and implicates a bursty frameshifting mechanism. Besides frameshifting, our technology can now be used to examine other translational regulatory dynamics, including upstream open reading frame selection, non-canonical initiation, and ribosomal shunting. In particular, the high spatiotemporal resolution of our technology makes it possible to detect and quantify even the smallest sub-populations of translating RNA. Whereas ribosome profiling (Ingolia et al., 2009) and single-cell assays (Han et al., 2014) can provide detailed snapshots of the average translational state of a cell, they lack the spatiotemporal

Please cite this article in press as: Lyon et al., Live-Cell Single RNA Imaging Reveals Bursts of Translational Frameshifting, Molecular Cell (2019), https://doi.org/10.1016/j.molcel.2019.05.002

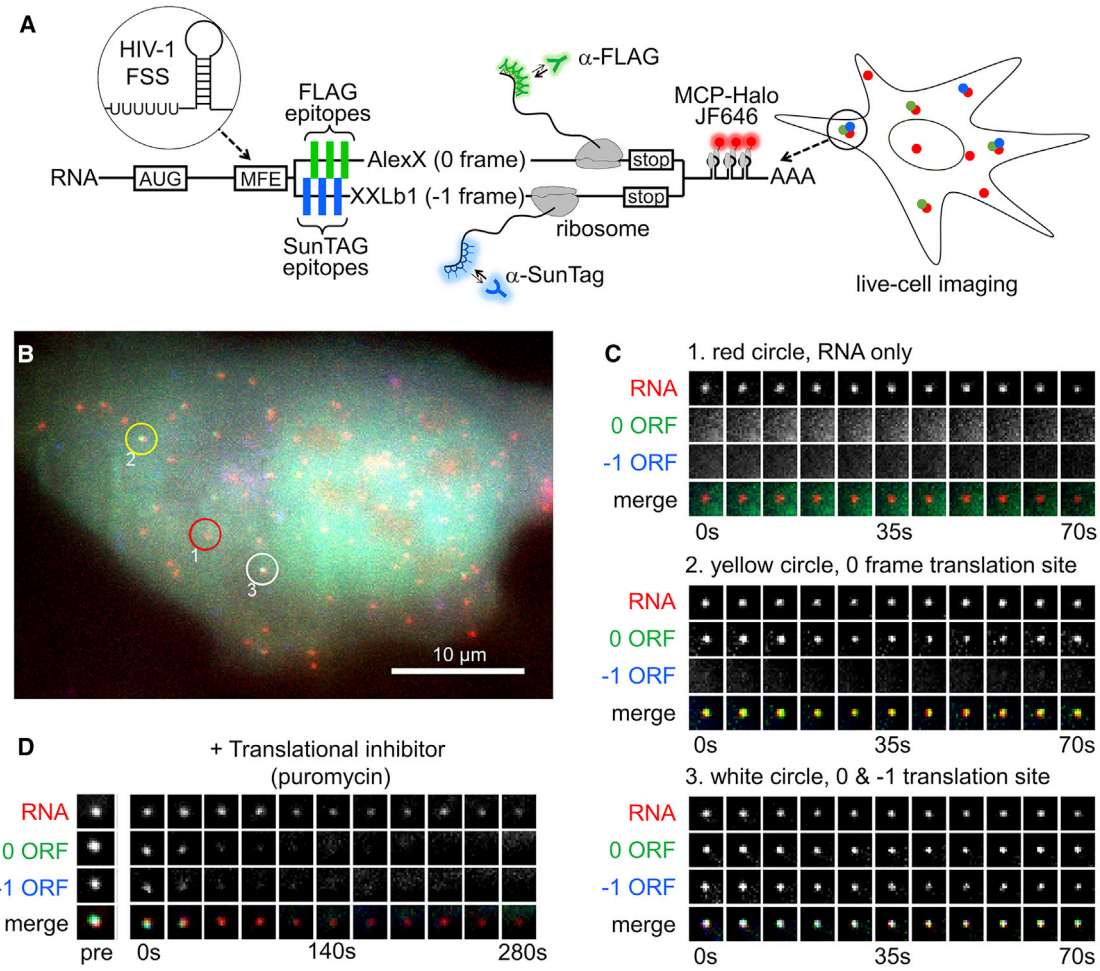

Figure 1. A Multi-Frame Tag to Image Single RNA Frameshifting Dynamics in Living Cells

(A) The multi-frame (MF) tag contains 12 repeated FLAG epitopes in the 0 frame interspaced between 12 repeated SunTag v4 epitopes in the –1 frame. Depending on which frame is translated, nascent epitopes are labeled by fluorescent α-FLAG antibody fragments (Cy3-Fab, green "Y") or α-SunTag single chain variable fragments (scFv-GFP, blue "Y"). Following the repeat epitopes is exon 1 of the GNAS locus, in which the peripheral membrane proteins AlexX (689 aa) and XXLb1 (690 aa) were placed in the 0 and −1 frames, respectively. Preceding the multi-frame tag is a multi-frame element (MFE). In this study, the HIV-1 frameshift sequence (FSS) was used as the MFE. To facilitate single-RNA tracking, a 24X MS2 stem-loop tag was also placed in the 3′ UTR. This tag is labeled by MCP-HaloTag (with JF646-HaloTag ligand, red).

(B) A representative cell ~10 h after transient transfection with the multi-frame tag depicted in (A). The red circle (labeled "1") highlights a non-translating RNA, the yellow circle (labeled "2") highlights a 0-frame translation site (TS), and the white circle (labeled "3") highlights a 0 and −1 TS. Scale bar, 10 μm.

(C) Montages showing the temporal evolution of the RNA spots circled in (B).

(D) A representative montage showing the loss of signal from the 0 and −1 open reading frames upon addition of the translational inhibitor puromycin (100 μg/mL).

See also Figure S1 and Videos S1 and S2.

resolution required to capture translation dynamics at the single-RNA level. We therefore anticipate multi-frame nascent chain tracking will be a powerful tool to dissect complex translational regulatory dynamics in living cells and organisms.

RESULTS

A Multi-Frame Tag to Monitor Single-RNA Translation in Two Reading Frames Simultaneously

We created a multi-frame (MF) tag to monitor, in living cells, the translation of single RNAs with overlapping open reading frames (ORFs). The tag builds off earlier technology to visualize translation using repeat FLAG or SunTag epitopes labeled by fluorescent Fab or scFv, respectively (Lyon and Stasevich, 2017; Morisaki and Stasevich, 2018). In the MF tag, FLAG epitopes in the 0 frame are separated from one another by SunTag epitopes in the −1 frame. With this arrangement, as shown in (Figure 1A), single RNAs with ribosomes translating the 0 frame will produce FLAG epitopes labeled by Fab (green), while those with ribosomes translating the −1 frame will produce SunTag epitopes labeled by scFv (blue). Thus, depending on the chosen frame(s), polysomes will appear all green (all ribosomes translating the 0 frame), all blue (all ribosomes translating the −1 frame), or some combination of the two.

To ensure both frames of the MF tag encode functional proteins and have similar coding sequence length, we inserted the first exon of the human GNAS locus downstream of the FLAG and SunTag epitopes. The GNAS locus contains two overlapping ORFs of roughly equivalent lengths that encode peripheral membrane proteins in the 0 and −1 frames: XXLb1 and AlexX (Abramowitz et al., 2004; Aydin et al., 2009; Figure 1A). In combination with the epitopes, this arrangement has several advantages. First, FLAG epitopes are interspersed between SunTag epitopes. Thus, when FLAG epitopes are translated, the out-of-frame SunTag epitopes act as linkers between consecutive FLAG epitopes (and vice versa). This is an optimal arrangement in that additional linkers between epitopes would further space them out and lower their density within the tag. Second, signals are digital, so frameshifted and non-frameshifted species are marked by two distinct probes/colors. Third, epitopes are placed in nearly equivalent positions, so signals appear at roughly the same time and with similar amplification when translated with similar kinetics.

As a first application of the MF tag, we focused on −1 programmed ribosomal frameshifting caused by the HIV-1 FSS. We inserted the FSS upstream of our MF tag and transiently transfected the resulting construct into U-2 OS cells. The FSS contains a slippery poly-U stretch nine nucleotides upstream of a stem loop. In the 2–10 h after transfection, we observed cells with tens or hundreds of individual RNA diffusing throughout the nucleus and cytoplasm (Figure 1B). Nascent chain tracking (NCT) (Morisaki et al., 2016) of the RNA revealed a high degree of RNA-to-RNA heterogeneity, with a subset of RNA labeled by Fab only—indicative of FLAG epitopes from translation in the 0 frame—and a smaller subset labeled by both Fab and scFv—indicative of both FLAG and SunTag epitopes from canonical and frameshifted translation in the 0 and −1 frames, respectively (Figures 1B and 1C; Video S1).

To confirm these RNA were active translation sites, or polysomes, we performed two experiments. First, we re-imaged cells 12–24 h after transfection. At these later time points, Fab and scFv began to accumulate in the cell membrane (Figure S1A, left panels), as would be expected if they labeled mature and functional XXLb1 and AlexX proteins (Aydin et al., 2009). In cells transfected with the −FSS control tag, little or no −1 frame product accumulation was observed (Figure S1A, middle panels), despite this frame encoding a functional protein, as demonstrated by shifting the sequence by one nucleotide into the 0 frame (Figure S1A, right panels). Second, we treated cells with the translational inhibitor puromycin. Just minutes after treatment, we observed a dramatic decrease in the number of Fab- and/or scFv-labeled RNA, consistent with the premature release of nascent chains (Figure 1D; Video S2, left). Together, these data provide strong evidence that we are able to detect single RNA frameshifting dynamics with the MF tag.

Using the MF Tag to Quantify HIV-1 Frameshifting Efficiency

The HIV-1 FSS structure has been previously shown to produce frameshifted protein with an efficiency of 5%–10% based on the dual luciferase assay and similar bulk assays (Brierley and Dos Ramos, 2006; Dulude et al., 2002; Grentzmann et al., 1998; Mouzakis et al., 2013). However, it remains unclear how this percentage is established. One possibility is that all RNA behave more or less the same and their ribosomes frameshift with 5%–10% probability. On the opposite end of the spectrum, it is possible that RNA display a high degree of heterogeneity, so that just 5%–10% of RNA have ribosomes that frameshift with nearly 100% probability. A third possibility is that frameshifting is common on all RNA, but frameshifted proteins are less stable and degraded faster than non-frameshifted proteins.

As a first step to quantify frameshifting dynamics at the single-molecule level, we tracked thousands of individual RNA ~2–10 h post transfection with and without the FSS sequence present (±FSS; Figures 2A–2C). We observed all possible types of translation sites (Figure S1B). In addition, we observed many non-translating RNA as well as mature protein puncta. These single-color spots served as convenient internal controls that demonstrated no fluorescence bleed-through at our imaging conditions (Figure S1B). In the +FSS cells we found 92% ± 1.3% of translation sites were translating the canonical 0 frame alone, while 6.2% ± 1.1% were translating both the 0 and −1 frames. Only rarely did we observe translation sites translating just the −1 frame (1.6% ± 0.5%) (Figures S1B and S2A). To ensure these results were not influenced by the MF tag, we reversed the FLAG and SunTag epitopes in the tag. Repeating the experiments with the reversed tag yielded the same fraction of translating and frameshifting RNA ($p = 0.18$ and 0.46, respectively) (Figure S2C), confirming the tag order and/or epitope positioning did not bias measurements. The consistency also suggests we are able to detect all or nearly all translation sites with either tag. We then repeated experiments in cells transfected with the −FSS control tag. In this case, we observed virtually no frameshifting sites (0.9% ± 0.7%) (Figures 2B, 2C, and S2B). Taken together, these data suggest the FSS alone causes ~8% of translation sites to frameshift.

To further characterize the efficiency of frameshifting, we quantified the number of frameshifted versus non-frameshifted nascent chains (or ribosomes) per translation site. To do so, we imaged a calibration reporter harboring a single FLAG or single SunTag epitope, but otherwise identical in length and sequence to the −FSS control tag (Figures S2D–S2I). With the calibration construct, each nascent chain in a translation site is labeled by a single fluorophore. Because the fluorescence of a single fluorophore can be unambiguously measured via the observation of single-step photobleaching, the ratio of translation site fluorescence to single-fluorophore fluorescence provides a good estimate for the number of nascent chains (in units of mature protein). After calibrating the +FSS MF tag, we found 0-frame only sites had 6.1 ± 0.2 nascent chains (versus 9.3 ± 0.3 for the −FSS control tag), 0- and −1-frame sites had 11.4 ± 1.6 nascent chains total, 2.8 ± 0.5 of which were frameshifted, and −1-frame only sites had 5 ± 2 frameshifted nascent chains (Figure 2D). Thus, although just ~8% of translation sites contained frameshifted nascent chains, within this subset of sites, a relatively large fraction of nascent chains were frameshifted, anywhere between 25% (in 0- and −1-frame translation sites) to 100% (in −1-frame only translation sites). Together, these data support a heterogeneous RNA model in which frameshifting occurs on a small subset of RNA with high probability.

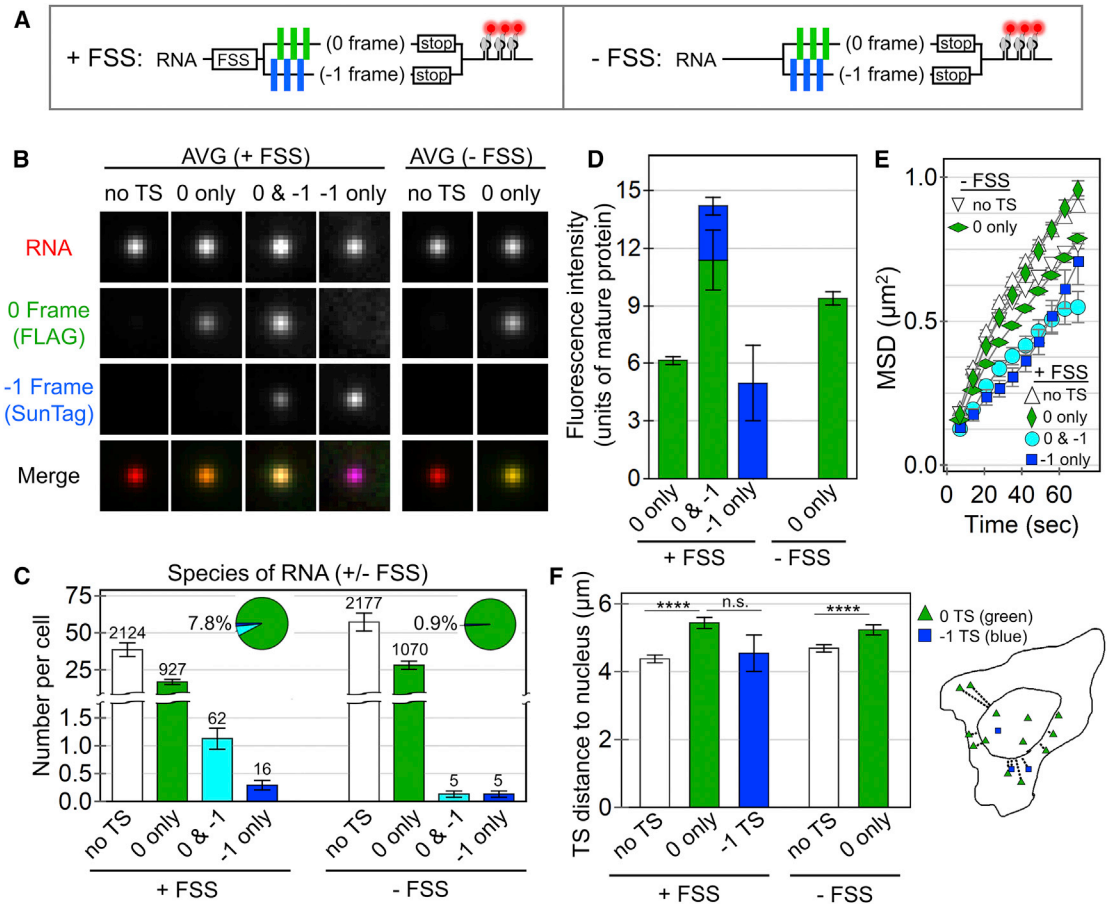

Figure 2. Quantification of HIV-1 Stimulated Frameshifting

(A) A schematic of the MF (+FSS) and control (−FSS) tags.

(B) Average image trims of all non-translating RNA sites (no TS), 0-frame only translation sites (0 only), 0- and −1-frame translation sites (0 and −1), and −1-frame only translation sites (−1 only), with their respective merges.

(C) The number of cytosolic and nuclear RNA detected per cell transfected with either the +FSS MF tag (60 cells, 3,129 total RNA) or the −FSS control tag (49 cells, 3,257 total RNA). The pie charts highlight the percentage of all frameshifting species per transfected cell. The number of detected RNA for each species is shown above each bar. Error bars represent SEM among cells.

(D) The fluorescence intensity (in units of mature protein) of nascent chains per translation site for the +FSS MF and −FSS control tags. Error bars represent SEM among RNA.

(E) The mean squared displacement (MSD) of tracked RNA species as a function of time. Error bar represent SEM among RNA. The diffusion coefficient (D_{RNA}) was estimated from a linear fit to the first four time points (95% confidence interval [CI]). For the +FSS MF tag: no TS (D_{RNA} = (1.8 ± 0.09) × 10^{-2} μm²/s); 0 only (D_{RNA} = (1.6 ± 0.06) × 10^{-2} μm²/s); 0 and −1 (D_{RNA} = (1.0 ± 0.04) × 10^{-2} μm²/s); and −1 only (D_{RNA} = (0.7 ± 0.06) × 10^{-2} μm²/s). For the –FSS control tag: no TS (D_{RNA} = (1.6 ± 0.1) × 10^{-2} μm²/s); and 0 only (D_{RNA} = 1.3 ± 0.07 × 10^{-2} μm²/s).

(F) The average distance (μm) of detected translation sites from the nucleus. Error bars represent SEM among RNA. An outline of a representative cell on the right shows all detected translating RNA within the cell and their measured distance from the nuclear border (inner curve). p values are based on the Mann-Whitney U test; *p < 0.05; **p < 0.01; ***p < 0.001; ****p < 0.0001.

See also Figure S2.

Characterizing the Mobility, Location, and Local Environment of Frameshifting

Given the heterogeneity of observed frameshifting, we hypothesized that the frameshifting state could be stimulated by a specific sub-cellular environment. To test this hypothesis, we performed a statistical analysis of all tracks to see if any biophysical parameters correlated with frameshifting. This revealed frameshifting sites diffuse more slowly than other translation sites or RNA (p < 0.05, Figure 2E). This could be due to a preference for frameshifting in the peri-nuclear endoplasmic reticulum, where RNA have been shown to be less mobile and more efficiently translated (Voigt et al., 2017; Wang et al., 2016). In contrast to this, we did not find a preference for frameshifting RNA to be closer to the nucleus compared to non-frameshifting RNA (p = 0.21, Figure 2F).

Of the parameters we quantified, one of the strongest correlates of frameshifting was RNA signal intensity. Specifically, sites translating both the 0 and −1 frames had an average RNA signal intensity that was nearly 30% brighter than RNA-only spots (Figures 2B and S3A). This was not due to a few outliers, as >80% of all such

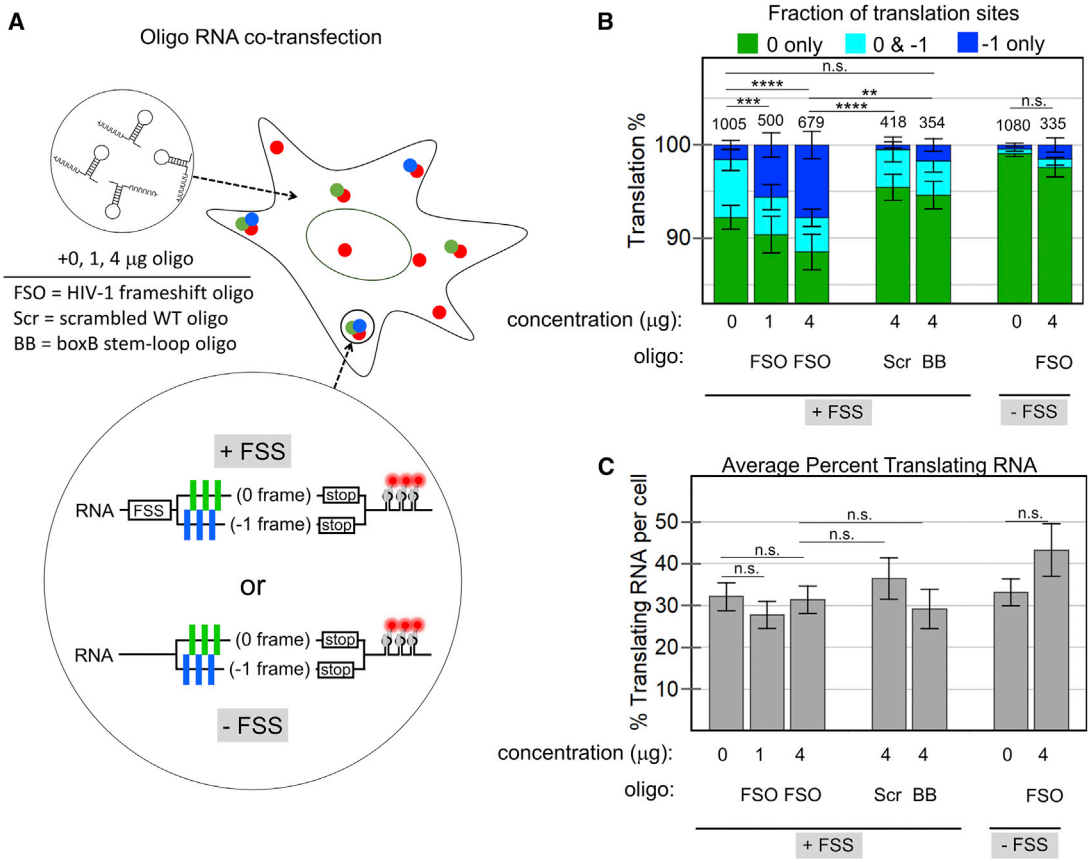

Figure 3. Frameshifting Can Be Stimulated by an Oligo Encoding the FSS

(A) Cells were co-transfected with different concentrations of short oligo RNAs encoding just the FSS (FSO), a scrambled FSO sequence (Scr), or the boxB stem-loop sequence (BB), together with either the +FSS MF tag or −FSS control tag.

(B) The percentage of translation sites translating just the 0 frame only (green, 0 only), the 0 and −1 frames (cyan, 0 and −1), or just the −1 only frame (dark blue, −1 only). Below each plot the concentration of loaded oligo (0, 1, or 4 μg), oligo type (FSO, Scr, or BB), and construct (+FSS or −FSS) are indicated.

(C) Average percentage of translating RNA per cell for the experiments in (B). The error represents SEM between cells. The p values are based on the Mann-Whitney U test of −1 frame percentages between experiments; *$p < 0.05$; **$p < 0.01$; ***$p < 0.001$; ****$p < 0.0001$.

See also Figure S3 and Video S2.

translation sites had above average RNA signal intensities (Figure S3B). Because these sites have nearly twice as many nascent chains as other sites (Figure 2D), it is likely they contain multiple translating RNA. To corroborate this, we chose the 50% dimmest RNA (which are presumably single RNA). In this gated RNA subpopulation, the intensity distribution of the 0-frame nascent chains got significantly dimmer for 0- and −1-frameshifting sites ($p = 0.037$; Figure S3B). In contrast, the intensity distributions of the 0 frame only and −1 frame only spots did not change significantly upon gating (Figure S3B, $p = 0.89$ and 0.71, respectively). These data imply frameshifting sites are often composed of two (or more) translating RNAs, at least one of which is frameshifting.

We wondered if the multi-RNA frameshifting sites were an artifact due to the aggregation of probes. Self-aggregation of Fab was unlikely as this would cause 0-frame translation sites to be just as bright −1-frame translation sites, which was not the case for both the +FSS MF tag and the −FSS control tag (Figures S3A and S3C, $p < 0.0001$ in both cases). Similarly, it was unlikely to be due to self-aggregation of scFv, as this would cause 0-frame translation sites to be just as bright as −1-frame translation sites in the reverse MF tag (with SunTag epitopes in the 0 frame), which was also not the case (Figure S3D, $p < 0.0001$). This left the possibility that Fab aggregate with scFv. To rule this out, we reimaged the MF tag without Fab. As frameshifting translation sites still had brighter RNA signal intensities than other sites (Figure S3E, $p < 0.0001$), we conclude the brighter signal is not a tagging artifact, but instead represents a propensity for frameshifting RNA to associate with other RNA to form higher-order multimer sites. Indeed, although difficult to capture, we have observed such multimers dissociate upon puromycin treatment (Video S2, right).

Frameshifting Can Be Stimulated by an Oligo Encoding the FSS

Unlike experiments with the +FSS MF tag, we did not observe a significant number of translation sites with increased RNA signal intensity in experiments with the −FSS control tag (compare Figure S3A to S3C, 0 only $p < 0.01$; −1 TS $p < 0.001$). We therefore

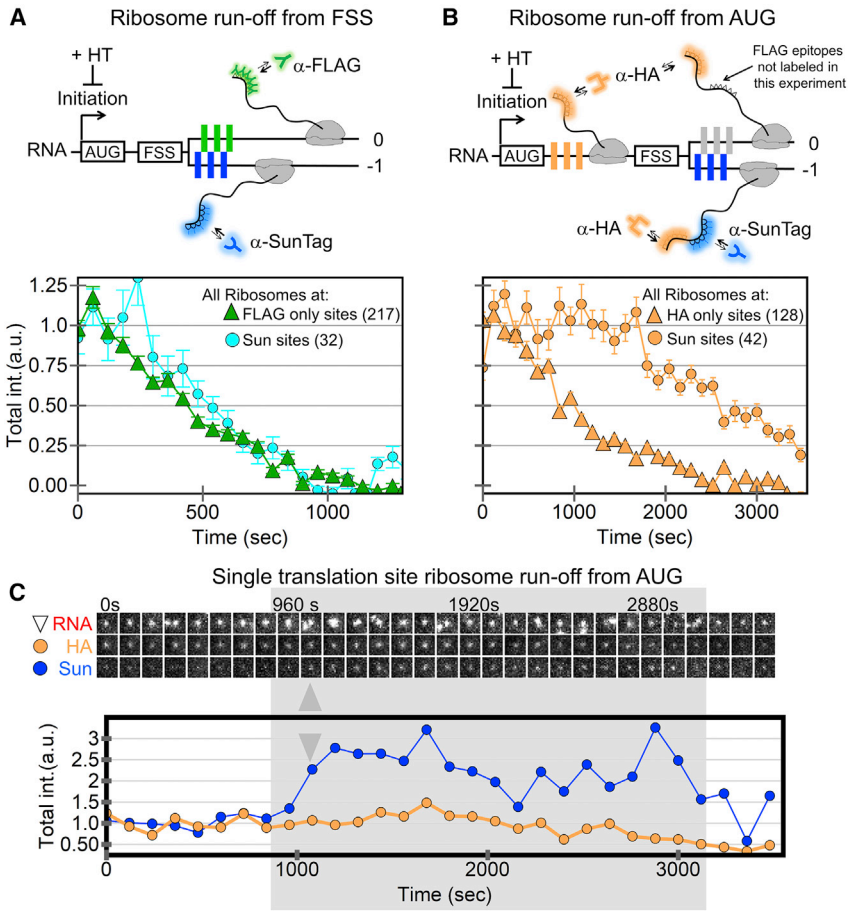

Figure 4. Ribosomal Run-Off at Frameshifting and Non-frameshifting Translation Sites

(A) A schematic showing harringtonine-induced ribosomal run-off from the +FSS 2xMF tag with FLAG (green) and SunTag epitopes (blue) in the 0 and −1 frames, respectively. The normalized total intensity (a.u.) of nascent chain signals within non-frameshifting translation sites (green triangles, 217 FLAG-only sites initially) and frameshifting sites (cyan circles, 32 Sun sites initially). Frameshifting translation sites are distinguished by the presence of α-SunTag scFv. As these sites contain both FLAG and SunTag nascent chains, the intensity is the sum of the α-FLAG Fab and α-SunTag scFv fluorescence. There is a small but significant difference between the run-off of non-frameshifting versus frameshifting ribosomes ($p < 0.001$ for all time points up to ~600 s, after which the two curves begin to converge to zero intensity, Mann-Whitney U test, 19 cells). Error bars represent SEM of all sites.

(B) Similar to (A), but with a modified MF tag with the addition of 10 HA epitopes (orange, HA MF tag) upstream of the FSS. The α-HA Fab signals in non-frameshifting translation sites (orange triangles, 128 HA-only sites initially) and frameshifting translation sites (orange circles, 42 Sun sites initially). Frameshifting translation sites are distinguished by the presence of α-SunTag scFv. The non-frameshifting and frameshifting HA run-offs were significantly different ($p < 0.0001$ for all time points, Mann-Whitney U test, 27 cells). Error bars represent SEM of all sites.

(C) A sample single translation site encoding the modified HA MF tag (shown in B) after addition of harringtonine. A montage of image trims shows the detected RNA-, HA-, and Sun-signals through time. Below, the normalized total intensity of the α-HA Fab signal (marking all ribosomes) and the α-SunTag scFv signal (marking frameshifting ribosomes) is plotted through time. Gray arrows and gray box signify a burst of frameshifting.

See also Figure S4 and Video S3.

hypothesized the FSS sequence could be involved in multimerization. To test this, we co-transfected cells expressing the +FSS MF tag with a short oligo RNA encoding just the FSS sequence (FSO; frameshift oligo, Figure 3A). Remarkably, this led to a significant increase in the fraction of frameshifting sites translating just the −1 frame, from 1.6% to 5.6% when 1 μg FSO was added (Figure 3B, $p < 0.001$), and up to 7.8% when 4 μg FSO was added ($p < 0.0001$, Figure 3B). However, in contrast to our expectation, the FSO did not significantly impact the RNA signal intensities within frameshifting sites. Instead, irrespective of FSO concentration, the distributions of RNA signal intensities within frameshifting (and non-frameshifting) sites remained statistically unchanged (Figures S3F and S3G). For controls, we repeated experiments, first with non-specific oligos and second with the FSO in cells expressing the −FSS control tag. In both cases, we did not see a significant increase in frameshifting (Figure 3B). Furthermore, in all experiments the fraction of translating RNA remained statistically constant (Figure 3C), indicating cellular stress was not a factor. We therefore conclude the FSS can somehow interact with other translation sites to facilitate frameshifting. While it remains unclear if the interaction is direct or indirect, by itself the interaction does not appear to alter the multimerization of frameshifting sites.

Translational Output of Frameshifted Ribosomes

The ~8% of frameshifted translation sites we observed is consistent with previous measurements of 5%–10% frameshifted protein product (Brierley and Dos Ramos, 2006; Dulude et al., 2002; Grentzmann et al., 1998; Mouzakis et al., 2013). All else equal, this implies that frameshifting alone can explain the steady-state levels of frameshifted protein, without the need for other regulatory mechanisms, such as protein degradation. To test this hypothesis, we performed a ribosomal run-off experiment to roughly estimate the elongation rates of frameshifted and non-frameshifted ribosomes. We used a doubled +FSS MF tag (2xMF tag) to increase the signal amplification. This allowed us to lower the laser powers and thereby eliminate observable photobleaching. Fits to the post-tag portion of run-off curves yielded similar run-off times (Figures 4A and S4A). Fluorescence recovery after photobleaching experiments further

confirmed these estimates without the use of translation inhibitors (Figure S4B). Based on these similar post-tag elongation rates, a single round of translation would take ~9 min, irrespective of frameshifting. Accounting for the number of ribosomes per translation site and their relative fractions, we calculate a cell with 100 RNA would produce ~170 frameshifted protein per hour compared to ~4,200 canonical proteins. In other words, frameshifted proteins would account for ~4% ± 1% of the total, in agreement with earlier measurements. Thus, the FSS sequence alone can be sufficient to account for the steady-state levels of frameshifted protein in living cells, without the need for additional regulatory mechanisms.

Evidence for Ribosomal Traffic Jams at HIV-1 Frameshifting Translation Sites

Despite the similar elongation rates, we noticed a slight but significant delay in the run-off response at frameshifting translation sites compared to non-frameshifting translation sites (compare "Sun sites" to "FLAG only sites" in Figure 4A, $p < 0.001$). Given earlier work showing the potential of the FSS to pause ribosomes (Dulude et al., 2002), we envisioned this delay could be due to a queue or traffic jam of ribosomes upstream of the FSS. As the backed-up ribosomes clear the traffic jam, they replenish the loss of ribosomes running-off. Only after the traffic jam is fully cleared does the number of ribosomes beyond the FSS (with labeled nascent chains) begin to decay. Consistent with this notion, a ribosomal traffic jam upstream of the FSS would make it appear like there are fewer ribosomes per transcript compared to the −FSS control tag, as we observed (Figure 2D).

To more directly test for ribosomal traffic jams, we added a 10x HA epitope repeat upstream of the +FSS MF tag (creating the HA MF tag, Figure 4B). This served two purposes: first, it allowed us to monitor both ribosomes upstream of the FSS (translating HA epitopes) and ribosomes downstream (translating either 0-frame FLAG or −1-frame SunTag epitopes); second, the arrangement more closely mimicked the natural placement of the FSS between the Gag-Pol polyproteins. In particular, the HA MF tag includes 368 codons upstream of the FSS compared to just 23 codons with the original +FSS MF tag. This extra space could theoretically accommodate longer ribosomal traffic jams (up to ~40 ribosomes), should they occur. We hypothesized that longer ribosomal traffic jams would lead to longer run-off delays. Consistent with this, ribosomes within frameshifting sites took much longer to run-off compared to ribosomes in non-frameshifting sites (compare "Sun sites" to "HA only sites" in Figure 4B, $p < 0.0001$), with frameshifted ribosome levels remaining high for upward of 3,000 s, despite an overall ribosome loss (Figures S4C and S4D). We observed this trend even at the single-molecule level, where the fluorescence signal intensity of HA (marking all ribosomes) decreased through time, but the fluorescence signal intensity of SunTag (marking only the frameshifted ribosomes) fluctuated through time (Figures 4C and S4F; Video S3). These fluctuations reflect the stochastic release of stalled ribosomes within the traffic jam. Such a release can be seen in the single-molecule track at the ~1,000 s time point, when the frameshift signal gets significantly brighter. Although difficult to capture, we observed this type of dynamic in another single frameshifting RNA track as well (Figures S4E and S4F).

Computational Modeling of HIV-1 Frameshifting Bursts at the Single RNA Level

To quantify the kinetics of frameshifting, we developed two candidate models and attempted to fit each to our four main observations: (1) the percentages of single RNA engaged in 0 frame, −1 frame, and both frame translation, (2) nascent chain intensities in 0 and/or −1 frames on these RNA, (3) the average total ratio of −1 frame to 0 frame protein production, and (4) run-off kinetics for original and extended HA constructs. To disentangle effects of single-RNA translation and aggregation of translating RNA to form translation site multimers, we down-selected to the 50% dimmest RNA (Figure S3B) before fitting items (1) and (2). We reiterate that gating on the dimmest RNA led to no significant difference for the intensities of 0 only or −1 only translation sites, but removed 80% of the 0- and −1-frame translation sites, providing more evidence that these spots are multiple RNA. Items (3) and (4) refer to the total 0 and −1 frame translation and were fit without gating.

Both models include initiation of ribosomes, codon-dependent elongation of proteins along the RNA template, and ribosomal exclusion to block ribosomes from passing or occupying the same place on the RNA. The only difference in the two models is the treatment for how ribosomes shift from the 0 to the −1 frame. The first model assumes constitutive frameshifting, in which each ribosome can frameshift at the FSS with a fixed and equal probability. This model could capture either observation (1) or (2), but not both simultaneously; frameshifting either led to excessively large fractions of frameshifting sites or excessively small ribosomal loading, in disagreement with our observations that a relatively small fraction of RNA frameshift with relatively high ribosomal occupancies. Even with addition of distinct pauses in elongation at the FSS in both frames, the constitutive model was unable to fit our data (Figures S5A–S5L).

The second model is inspired by two-state gene models that are commonly used to describe heterogeneous transcription (Munsky et al., 2012). In this "bursty" model, RNA stochastically switch between non-frameshifting and frameshifting states in which either 0% or 100% of ribosomes produce frameshifted proteins (Figure 5A). In the bursty model, the RNA frameshift state is assumed to switch ON and OFF at rates k_{on} and k_{off}, respectively, and the steady-state fraction of RNA in the ON state is given by $f = k_{on}/(k_{on} + k_{off})$.

To estimate the timescale of switching (k_{off}), we tracked translation sites for longer periods of time. To achieve this tracking, we used the brighter +FSS 2xMF tag and changed our imaging strategy to sample the RNA signal intensity at all time points and the 0 and −1 translation signals once every fifth time point. This arrangement substantially reduced photobleaching and allowed us to continuously track and monitor the translational status of single translation sites in 3D for nearly an hour. Figure 5B shows the frameshifting state survival times for the seven translation sites we tracked in this manner, including one site that frameshifted for longer than 40 min (Figure S5M; Video S4), representing at least four rounds of translation at our estimated elongation rate. Remarkably, this frameshifting translation site associated with another for a large part of the 40-min imaging window. This supports the notion that the brighter RNA signal intensity at frameshifting sites comes from more than one RNA. From

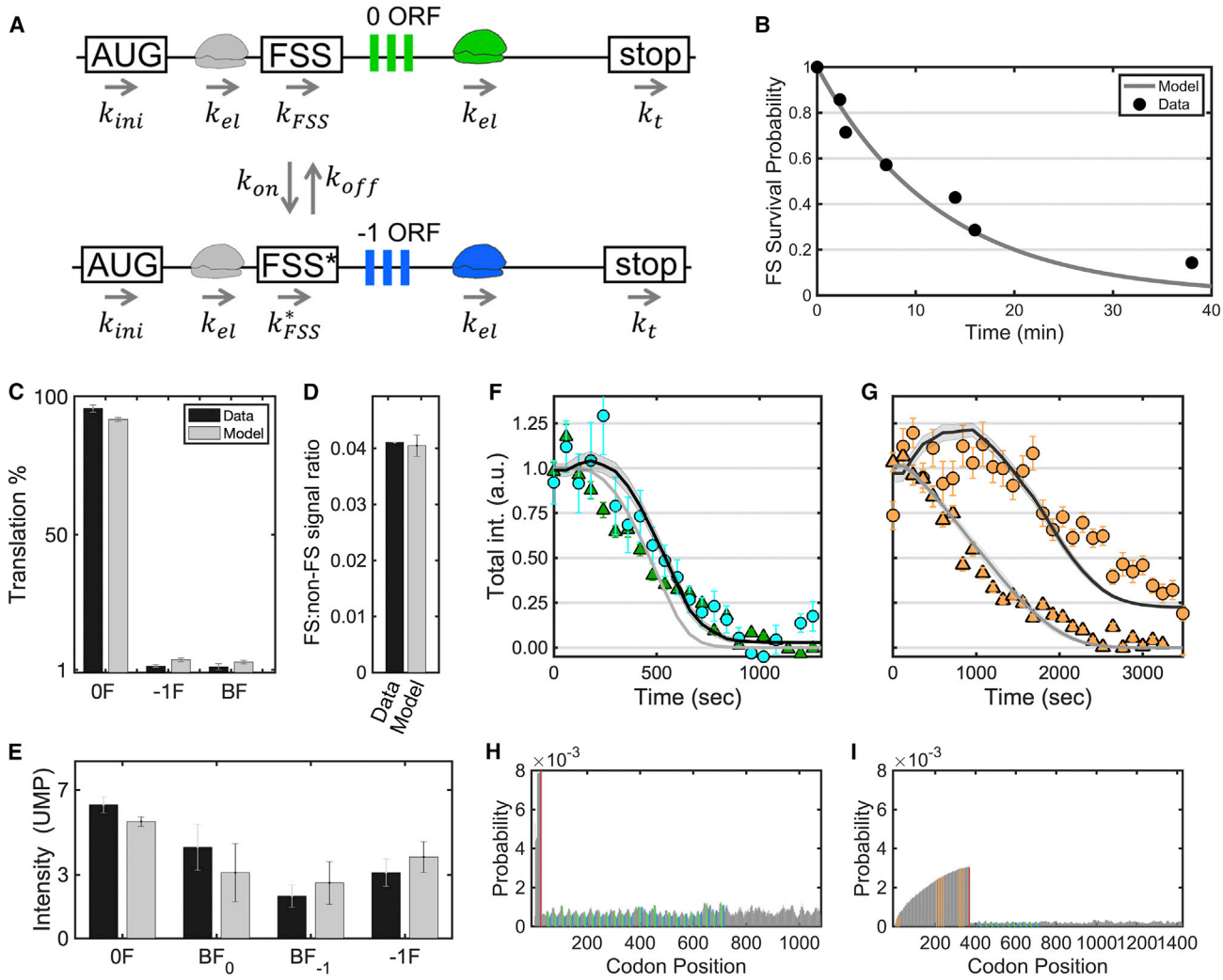

Figure 5. A Model for Bursty Frameshifting

(A) A schematic of the model: k_{ini} is the translation initiation rate, k_{el} is the translation elongation rate, k_{on} is the rate at which RNA switch to the frameshifting state, k_{off} is the rate at which RNA switch to the non-frameshifting state, k_{FSS} is the pause rate at the FSS in the non-frameshifting state, k^*_{FSS} is the pause rate at the FSS in the frameshifting state, and k_t is the termination rate (assumed equal to k_{el}).

(B) The survival probability of frameshifting sites through time (black dots) is fit with a single exponential decay (gray line).

(C–G) Simultaneous fit of all data. (C) A bar graph comparing the measured (black) and best-fit model predicted (gray) percentage of non-frameshifting (0F), frameshifting (−1F), and both frames (BF) translation sites. Error bars represent SEM among cells. (D) A bar graph comparing the measured (black) and best-fit model predicted (gray) ratio between the total frameshifted and non-frameshifted signal intensity (FS:non-FS signal ratio). (E) A bar graph comparing the measured (black) and best-fit model predicted (gray) intensity in units of mature protein (u.m.p.) within non-frameshifting (0F), frameshifting (−1F), and both frames (BF) translation sites. Error bars represent SEM among RNA. (F) Best-fit model (solid lines) of the data from Figure 4A. Error bars represent SEM among RNA. (G) Best-fit model prediction of the data from Figure 4B. Error bars represent SEM among RNA.

(H) The predicted ribosomal occupancy along the MF tag is shown. The positions of the FSS (red), FLAG (green), and SunTag (blue) epitopes are shown in color.

(I) The predicted ribosomal occupancy along the HA MF tag is shown. The positions of the FSS (red), HA (orange), FLAG (green), and SunTag (blue) epitopes are shown in color.

See also Figure S5 and Videos S4, S5, and S6.

the frameshift state survival times, we fit the rate of k_{off} to be ~0.0013 s^{-1} (Figure 5B), corresponding to an average frameshift persistence time of $1/k_{off}$ ~12.8 min.

Using this constrained value for k_{off}, we then fit to find the remaining parameters k_{on}, k_{ini}, k_{el}, k_{FSS}, and k_{FSS}^* (Table 1), with which the bursty frameshifting model could simultaneously reproduce all of our observations (Figures 5C–5G), in contrast to the constitutive model (Figures S5A–S5L). From these parameters, we calculate $1/k_{on}$ ~170 min, meaning that RNA encoding the HIV-1 FSS switch to a frameshifting state rarely, on the timescale of a few hours (Table 1, $1/k_{on}$). Once an RNA is in the frameshifting state, it remains there for tens of minutes on average (Table 1, $1/k_{off}$), occasionally lasting up to an hour or more. To account for the different run-off delays seen at frameshifting and

Table 1. Bursty Frameshifting Model Parameters and Calculated Quantities

Bursty Frameshifting Model Parameters from Simultaneous Fit	
Ribosome elongation rate k_{el}	3 ± 0.15 aa/s
Ribosome initiation rate k_{ini}	0.0244 ± 0.0015 s^{-1}
Switching on rate to frameshifting state k_{on}	$9.6 \times 10^{-5} \pm 7.8 \times 10^{-5}$ s^{-1}
Switching off rate from frameshifting state k_{off}	$1.3 \times 10^{-3} \pm 3.5 \times 10^{-4}$ s^{-1}
Pause rate at FSS in non-frameshifting state k_{FSS}	0.0234 ± 0.0012 aa/s
Pause rate at FSS* in frameshifting state k^*_{FSS}	0.0139 ± 0.0011 aa/s
Calculated Quantities for Bursting Model with HA MF Tag	
Fraction of frameshifted RNA	7% ± 5%
Average time in the non-shifting state $<b>$	170 ± 140 min
Average burst time in the shifting state $<b^*>$	12.8 ± 3.5 min
Number of ribosomes to initiate in a shifting state r^*_i	19 ± 5
Number of ribosomes to initiate in a non-shifting state r_i	250 ± 200
Time for a ribosome in shifting state to clear the FSS τ^*_{FSS}	75 ± 6 s
Time for a ribosome in non-shifting state to clear the FSS τ_{FSS}	46 ± 2 s

A summary of all fitted model parameters, along with a selection of quantities that can be calculated from the fitted parameters. The calculation details can be found in the STAR Methods. Note: formulas given in the STAR Methods.

non-frameshifting sites (Figures 5F and 5G), the model required elongation pauses of $1/k_{FSS} \sim 43$ s at non-frameshifting sites and $1/k^*_{FSS} \sim 72$ s at frameshifting sites. We explored if codon usage could also explain the differences in run-off times. However, according to the codon adaptation index (Gorgoni et al., 2016; Sharp and Li, 1987), which is related to the speed at which each codon is translated in the simulation, there is no notable difference between the 0 and −1 frames (Figure S5N). Moreover, the distinct pauses predicted by the model are comparable to those previously measured using *in vitro* and *in vivo* bulk assays (Chen et al., 2014; Lopinski et al., 2000).

Because the estimated average pause time, $1/k^*_{FSS}$, is greater than the average initiation time, $1/k_{ini}$, ribosomes could initiate faster than they clear the FSS with an excess rate of $k_{ini} - k^*_{FSS} = 0.011$ per s and create upstream traffic jams in frameshifting sites. These traffic jams would continue to build for as long as the RNA remains in the frameshifted state, or $\sim 1/k_{off} = 12.8$ min on average. Occasionally, traffic jams can extend all the way back to the start codon, as seen in a sample simulation (Figures 5H and 5I; Video S5). Moreover, due to the long time it can take to clear traffic jams, frameshifting can persist for hours following the global shut down of translation initiation (with harringtonine, for example), as can be seen in simulations of the best-fit model (Video S6) and consistent with what we observed in Figures 4C and S4E. Thus, the final bursty model suggests a mechanism by which frameshifting can persist for long periods in the absence of translation initiation.

DISCUSSION

Frameshifting is a common tactic used by viruses to minimize their genomes for faster, more efficient replication in host cells, effectively getting two viral proteins for the price of one viral RNA. While the general architecture of FSSs is well characterized and the dynamics of frameshifting have been measured with single-nucleotide precision *in vitro*, until now frameshifting had not been directly observed in a living system. To achieve this, we created a multi-frame repeat epitope tag that can light up single RNA translation sites in different colors depending on which open reading frame is being translated. Together with sensitive single-molecule microscopy and computational modeling, we have demonstrated six aspects of HIV-1 frameshifting: (1) frameshifted proteins originate from a small subset of RNA that frameshift with high efficiency; (2) frameshifting occurs in bursts on single RNA that can last for several rounds of translation; (3) ribosomes that frameshift are paused for longer at the frameshifting sequence than ribosomes that do not frameshift; (4) pauses at the FSS induce ribosomal traffic jams that can maintain the production of frameshifted protein despite global inhibition of translation; (5) frameshifting RNAs have reduced mobility and are often found in multi-RNA translation sites; and (6) frameshifting can be stimulated by an oligo encoding the FSS.

In contrast to constitutive frameshifting on any RNA, our data indicate that frameshifting occurs in bursts on a subset of RNA. Bursty expression has been demonstrated by others, both at single transcription sites as well as at translation sites in bacteria (Lionnet and Singer, 2012) and eukaryotes (Wu et al., 2016). The origin of frameshifting bursts is difficult to pinpoint. It is tempting to speculate that there is a unique structure the RNA takes that enhances frameshifting, particularly given the distinct pause times in our best-fit model. How this precisely occurs remains unclear, but our observation that the FSO (frameshift oligo) alone can stimulate frameshifting may offer some clues. In particular, this observation is consistent with the recently discovered repressor of frameshifting, shiftless (Wang et al., 2019). Shiftless is thought to directly bind the FSS sequence and cause frameshifted ribosomes to be prematurely released. The FSO would presumably sequester shiftless and thereby indirectly lead to an increase in frameshifting globally. More generally, the destabilization or unbinding of shiftless from the FSS could be responsible for the bursts of frameshifting we observed. These possibilities will be interesting to explore in the future.

According to our best-fit model, pauses always occur at the FSS, with longer pauses associated with frameshifting RNA compared to non-frameshifting RNA. Pausing is therefore only a weak predictor of frameshifting, as others have shown (Kontos et al., 2001; Tu et al., 1992). Nevertheless, the longer pauses associated with frameshifting suggest the FSS can adopt more than one state or structure, similar to what has been shown *in vitro* with sequences encoding pseudoknots (Houck-Loomis et al., 2011). Longer pauses result in longer ribosomal traffic jams. Our model predicts these jams can extend all the way

back to the initiation site, involving up to ~40 ribosomes, as shown in Figure 5I. Our model predicts an elevated ribosomal occupancy as far back as ~400 codons from the FSS, a length that coincides almost perfectly with the length of the FSS-upstream sequence in HIV-1 Gag-Pol. This is not unprecedented, as ribosome profiling experiments have also found evidence for relatively high ribosomal densities as far back as the start codon of the Gag protein (Napthine et al., 2017). These data suggest the strength of the HIV-1 pause may have evolved to on occasion produce the longest possible traffic jams. As clearance of these traffic jams takes time, frameshifting can persist on RNA for hours despite a global shut-down of translation initiation. In effect, the jam acts like a battery that continually fuels the production of downstream frameshifted protein. This unique mechanism would allow viral proteins to continue to increase in numbers during cellular stress. An open question is how these long traffic jams manage to evade protein quality control (Joazeiro, 2017; Juszkiewicz and Hegde, 2017), which recently was shown to target the interface of collided ribosomes within ribosomal traffic jams (Juszkiewicz et al., 2018).

Beyond the imaging of HIV-1 translational frameshifting, the MF tag can now be used in a variety of other contexts. For example, it can immediately be used to investigate frameshifting dynamics along other viral RNA sequences, as well as frameshifting thought to occur along endogenous human RNA, such as PEG10 (Cardno et al., 2015). Likewise, the MF tag can be used to examine other non-canonical translation processes involving more than one open reading frame, including start-codon selection, leaky scanning, ribosomal shunting, and general translation fidelity. In fact, in an accompanying paper, a similar multi-frame tag was used to examine upstream and downstream open reading frame selection (Boersma et al., 2019). Like us, the authors also saw a high degree of heterogeneity between translating RNAs, with bursts of translation initiation in multiple open reading frames similar to the bursts of frameshifting we observed at the HIV-1 FSS. Translational heterogeneity may therefore be far more common than originally appreciated, particularly when it comes to non-canonical translation. We therefore believe multi-color single molecule imaging of both canonical and non-canonical translation will become a powerful tool for dissecting complex RNA regulatory dynamics in a variety of important contexts.

STAR★METHODS

Detailed methods are provided in the online version of this paper and include the following:

- KEY RESOURCES TABLE
- CONTACT FOR REAGENTS AND RESOURCE SHARING
- METHOD DETAILS
  - Plasmid Construction
  - Fab generation and dye-conjugation
  - MCP and scFv-sfGFP purification
  - Cell culture, transfection, and bead-loading
  - Single molecule tracking microscopy
  - Particle tracking
  - Calibrating translation site intensity
  - Translation Site Species Identification
  - Puromycin treatment
  - Oligo RNA co-transfection
  - Ribosome Run-Off Experiments and fits
  - Fluorescence recovery after photobleaching (FRAP)
  - Statistical Analyses
  - General aspects of modeling frameshift kinetics
  - Computational Details
  - Simulation details
- DATA AND SOFTWARE AVAILABILITY

SUPPLEMENTAL INFORMATION

Supplemental Information can be found online at https://doi.org/10.1016/j.molcel.2019.05.002.

ACKNOWLEDGMENTS

We thank Dr. Hataichanok (Mam) Scherman of the Colorado State University Protein Expression/Purification Facility and Amanda Koch for cloning and purification of the SunTag scFv-sfGFP and MCP-Halo. We thank all members of the Stasevich and Munsky labs for helpful discussion and comments. This work is supported by the W.M. Keck Foundation.

AUTHOR CONTRIBUTIONS

Conceptualization, T.J.S., K.L., and B.M.; Methodology, K.L., L.U.A., T.M., B.M., and T.J.S.; Software, K.L., L.U.A., T.M., B.M., and T.J.S.; Formal Analysis, K.L. and L.U.A.; Experimentation, K.L., T.M., and T.J.S.; Computational modeling, L.U.A. and B.M.; Resources, B.M. and T.J.S.; Writing, Review, & Editing, K.L., L.U.A., T.M., B.M., and T.J.S.; Supervision, B.M. and T.J.S.; Funding Acquisition, B.M. and T.J.S.

DECLARATION OF INTERESTS

The authors declare no competing interests.

Received: November 26, 2018
Revised: March 14, 2019
Accepted: April 30, 2019
Published: June 6, 2019

REFERENCES

Abramowitz, J., Grenet, D., Birnbaumer, M., Torres, H.N., and Birnbaumer, L. (2004). XLalphas, the extra-long form of the alpha-subunit of the Gs G protein, is significantly longer than suspected, and so is its companion Alex. Proc. Natl. Acad. Sci. USA *101*, 8366–8371.

Atkins, J.F., Loughran, G., Bhatt, P.R., Firth, A.E., and Baranov, P.V. (2016). Ribosomal frameshifting and transcriptional slippage: From genetic steganography and cryptography to adventitious use. Nucleic Acids Res. *44*, 7007–7078.

Aydin, C., Aytan, N., Mahon, M.J., Tawfeek, H.A.W., Kowall, N.W., Dedeoglu, A., and Bastepe, M. (2009). Extralarge XL(α)s (XXL(α)s), a variant of stimulatory G protein α-subunit (Gs(α)), is a distinct, membrane-anchored GNAS product that can mimic Gs(α). Endocrinology *150*, 3567–3575.

Belew, A.T., Meskauskas, A., Musalgaonkar, S., Advani, V.M., Sulima, S.O., Kasprzak, W.K., Shapiro, B.A., and Dinman, J.D. (2014). Ribosomal frameshifting in the CCR5 mRNA is regulated by miRNAs and the NMD pathway. Nature *512*, 265–269.

Boersma, S., Khuperkar, D., Verhagen, B.M.P., Sonneveld, S., Grimm, J.B., Lavis, L.D., and Tanenbaum, M.E. (2019). Multi-color single molecule imaging uncovers extensive heterogeneity in mRNA decoding. Cell *178*. Published online June 27, 2019. https://doi.org/10.1016/j.cell.2019.05.001.

Brierley, I., and Dos Ramos, F.J. (2006). Programmed ribosomal frameshifting in HIV-1 and the SARS-CoV. Virus Res. *119*, 29–42.

Brierley, I., Digard, P., and Stephen, C. (1989). Characterization of an Efficient Coronavirus Ribosomal Frameshifting Signal : Requirement for an RNA Pseudoknot. Cell *57*, 537–547.

Caliskan, N., Katunin, V.I., Belardinelli, R., Peske, F., and Rodnina, M.V. (2014). Programmed -1 frameshifting by kinetic partitioning during impeded translocation. Cell *157*, 1619–1631.

Caliskan, N., Peske, F., and Rodnina, M.V. (2015). Changed in translation: mRNA recoding by -1 programmed ribosomal frameshifting. Trends Biochem. Sci. *40*, 265–274.

Cardno, T.S., Shimaki, Y., Sleebs, B.E., Lackovic, K., Parisot, J.P., Moss, R.M., Crowe-McAuliffe, C., Mathew, S.F., Edgar, C.D., Kleffmann, T., and Tate, W.P. (2015). HIV-1 and Human PEG10 Frameshift Elements Are Functionally Distinct and Distinguished by Novel Small Molecule Modulators. PLoS ONE *10*, e0139036.

Charbonneau, J., Gendron, K., Ferbeyre, G., and Brakier-Gingras, L. (2012). The 5′ UTR of HIV-1 full-length mRNA and the Tat viral protein modulate the programmed -1 ribosomal frameshift that generates HIV-1 enzymes. RNA *18*, 519–529.

Chen, J., Petrov, A., Johansson, M., Tsai, A., O'Leary, S.E., and Puglisi, J.D. (2014). Dynamic pathways of -1 translational frameshifting. Nature *512*, 328–332.

Choi, M.R., Yoo, N.J., An, C.H., and Lee, S.H. (2015). Frameshift mutations in mammalian target of rapamycin pathway genes and their regional heterogeneity in sporadic colorectal cancers. Hum. Pathol. *46*, 753–760.

Clark, M.B., Jänicke, M., Gottesbühren, U., Kleffmann, T., Legge, M., Poole, E.S., and Tate, W.P. (2007). Mammalian gene PEG10 expresses two reading frames by high efficiency -1 frameshifting in embryonic-associated tissues. J. Biol. Chem. *282*, 37359–37369.

Dulude, D., Baril, M., and Brakier-Gingras, L. (2002). Characterization of the frameshift stimulatory signal controlling a programmed -1 ribosomal frameshift in the human immunodeficiency virus type 1. Nucleic Acids Res. *30*, 5094–5102.

Edelstein, A.D., Tsuchida, M.A., Amodaj, N., Pinkard, H., Vale, R.D., and Stuurman, N. (2014). Advanced methods of microscope control using μManager software. J. Biol. Methods *1*, 10.

Gillespie, D.T. (1976). A general method for numerically simulating the stochastic time evolution of coupled chemical reactions. J. Comput. Phys. *22*, 403–434.

Gorgoni, B., Ciandrini, L., McFarland, M.R., Romano, M.C., and Stansfield, I. (2016). Identification of the mRNA targets of tRNA-specific regulation using genome-wide simulation of translation. Nucleic Acids Res. *44*, 9231–9244.

Grentzmann, G., Ingram, J.A., Kelly, P.J., Gesteland, R.F., and Atkins, J.F. (1998). A dual-luciferase reporter system for studying recoding signals. RNA *4*, 479–486.

Grimm, J.B., English, B.P., Chen, J., Slaughter, J.P., Zhang, Z., Revyakin, A., Patel, R., Macklin, J.J., Normanno, D., Singer, R.H., et al. (2015). A general method to improve fluorophores for live-cell and single-molecule microscopy. Nat. Methods *12*, 244–250.

Guerrero, S., Batisse, J., Libre, C., Bernacchi, S., Marquet, R., and Paillart, J.C. (2015). HIV-1 replication and the cellular eukaryotic translation apparatus. Viruses *7*, 199–218.

Han, K., Jaimovich, A., Dey, G., Ruggero, D., Meyuhas, O., Sonenberg, N., and Meyer, T. (2014). Parallel measurement of dynamic changes in translation rates in single cells. Nat. Methods *11*, 86–93.

Hayashi-Takanaka, Y., Yamagata, K., Wakayama, T., Stasevich, T.J., Kainuma, T., Tsurimoto, T., Tachibana, M., Shinkai, Y., Kurumizaka, H., Nozaki, N., and Kimura, H. (2011). Tracking epigenetic histone modifications in single cells using Fab-based live endogenous modification labeling. Nucleic Acids Res. *39*, 6475–6488.

Hooke, R., and Jeeves, T.A. (1961). "Direct Search"' Solution of Numerical and Statistical Problems. J. Assoc. Comput. Mach. *8*, 212–229.

Houck-Loomis, B., Durney, M.A., Salguero, C., Shankar, N., Nagle, J.M., Goff, S.P., and D'Souza, V.M. (2011). An equilibrium-dependent retroviral mRNA switch regulates translational recoding. Nature *480*, 561–564.

Ingolia, N.T., Ghaemmaghami, S., Newman, J.R.S., and Weissman, J.S. (2009). Genome-Wide Analysis in Vivo of Translation with Nucleotide Resolution Using Ribosome Profiling. Science *324*, 218–223.

Joazeiro, C.A.P. (2017). Ribosomal Stalling During Translation: Providing Substrates for Ribosome-Associated Protein Quality Control. Annu. Rev. Cell Dev. Biol. *33*, 343–368.

Juszkiewicz, S., and Hegde, R.S. (2017). Initiation of Quality Control during Poly(A) Translation Requires Site-Specific Ribosome Ubiquitination. Mol. Cell *65*, 743–750.

Juszkiewicz, S., Chandrasekaran, V., Lin, Z., Kraatz, S., Ramakrishnan, V., and Hegde, R.S. (2018). ZNF598 Is a Quality Control Sensor of Collided Ribosomes. Mol. Cell *72*, 469–481.

Kontos, H., Napthine, S., and Brierley, I. (2001). Ribosomal pausing at a frameshifter RNA pseudoknot is sensitive to reading phase but shows little correlation with frameshift efficiency. Mol. Cell. Biol. *21*, 8657–8670.

Lionnet, T., and Singer, R.H. (2012). Transcription goes digital. EMBO Rep. *13*, 313–321.

Lopinski, J.D., Dinman, J.D., and Bruenn, J.A. (2000). Kinetics of ribosomal pausing during programmed -1 translational frameshifting. Mol. Cell. Biol. *20*, 1095–1103.

Lyon, K., and Stasevich, T.J. (2017). Imaging Translational and Post-Translational Gene Regulatory Dynamics in Living Cells with Antibody-Based Probes. Trends Genet. *33*, 322–335.

Meydan, S., Klepacki, D., Karthikeyan, S., Margus, T., Thomas, P., Jones, J.E., Khan, Y., Briggs, J., Dinman, J.D., Vázquez-Laslop, N., and Mankin, A.S. (2017). Programmed Ribosomal Frameshifting Generates a Copper Transporter and a Copper Chaperone from the Same Gene. Mol. Cell *65*, 207–219.

Morisaki, T., and Stasevich, T.J. (2018). Quantifying Single mRNA Translation Kinetics in Living Cells. Cold Spring Harb. Perspect. Biol. *10*, a032078.

Morisaki, T., Lyon, K., DeLuca, K.F., DeLuca, J.G., English, B.P., Zhang, Z., Lavis, L.D., Grimm, J.B., Viswanathan, S., Looger, L.L., et al. (2016). Real-time quantification of single RNA translation dynamics in living cells. Science *352*, 1425–1429.

Mouzakis, K.D., Lang, A.L., Vander Meulen, K.A., Easterday, P.D., and Butcher, S.E. (2013). HIV-1 frameshift efficiency is primarily determined by the stability of base pairs positioned at the mRNA entrance channel of the ribosome. Nucleic Acids Res. *41*, 1901–1913.

Munsky, B., Neuert, G., and van Oudenaarden, A. (2012). Using gene expression noise to understand gene regulation. Science *336*, 183–187.

Nakamura, Y., Gojobori, T., and Ikemura, T. (1999). Codon usage tabulated from the international DNA sequence databases; its status 1999. Nucleic Acids Res. *27*, 292.

Napthine, S., Ling, R., Finch, L.K., Jones, J.D., Bell, S., Brierley, I., and Firth, A.E. (2017). Protein-directed ribosomal frameshifting temporally regulates gene expression. Nat. Commun. *8*, 15582.

Ritchie, D.B., Tittle, C., Rezajooei, N., Rouleau, L., Cappellano, T.R., Sikkema, W., and Woodside, M.T. (2017). Folding Heterogeneity in HIV-1 Frameshifting Hairpin. Biophys. J. *112*, 368a.

Schindelin, J., Arganda-Carreras, I., Frise, E., Kaynig, V., Longair, M., Pietzsch, T., Preibisch, S., Rueden, C., Saalfeld, S., Schmid, B., et al. (2012). Fiji: an open-source platform for biological-image analysis. Nat. Methods *9*, 676–682.

Sharp, P.M., and Li, W.H. (1987). The codon Adaptation Index–a measure of directional synonymous codon usage bias, and its potential applications. Nucleic Acids Res. *15*, 1281–1295.

Tokunaga, M., Imamoto, N., and Sakata-Sogawa, K. (2008). Highly inclined thin illumination enables clear single-molecule imaging in cells. Nat. Methods *5*, 159–161.

Tu, C., Tzeng, T.H., and Bruenn, J.A. (1992). Ribosomal movement impeded at a pseudoknot required for frameshifting. Proc. Natl. Acad. Sci. USA *89*, 8636–8640.

Viswanathan, S., Williams, M.E., Bloss, E.B., Stasevich, T.J., Speer, C.M., Nern, A., Pfeiffer, B.D., Hooks, B.M., Li, W.P., English, B.P., et al. (2015). High-performance probes for light and electron microscopy. Nat. Methods *12*, 568–576.

Voigt, F., Zhang, H., Cui, X.A., Triebold, D., Liu, A.X., Eglinger, J., Lee, E.S., Chao, J.A., and Palazzo, A.F. (2017). Single-Molecule Quantification of Translation-Dependent Association of mRNAs with the Endoplasmic Reticulum. Cell Rep. *21*, 3740–3753.

Wang, C., Han, B., Zhou, R., and Zhuang, X. (2016). Real-Time Imaging of Translation on Single mRNA Transcripts in Live Cells. Cell *165*, 990–1001.

Wang, X., Xuan, Y., Han, Y., Ding, X., Ye, K., Yang, F., Gao, P., Goff, S.P., and Gao, G. (2019). Regulation of HIV-1 Gag-Pol Expression by Shiftless, an Inhibitor of Programmed -1 Ribosomal Frameshifting. Cell *176*, 625–635.

Wu, B., Eliscovich, C., Yoon, Y.J., and Singer, R.H. (2016). Translation dynamics of single mRNAs in live cells and neurons. Science *352*, 1430–1435.

Yordanova, M.M., Wu, C., Andreev, D.E., Sachs, M.S., and Atkins, J.F. (2015). A nascent peptide signal responsive to endogenous levels of polyamines acts to stimulate regulatory frameshifting on antizyme mRNA. J. Biol. Chem. *290*, 17863–17878.

STAR★METHODS

KEY RESOURCES TABLE

REAGENT or RESOURCE	SOURCE	IDENTIFIER
Antibodies		
Anti DYKDDDDK mouse IgG_{2b} monoclonal	Wako	Cat#012-22384; RRID: AB_10659717
Anti HA-7 IgG_1 mouse monoclonal	Sigma-Aldrich	Cat#H3663; RRID: AB_262051
Bacterial and Virus Strains		
NEB® Stable Competent *E. coli*	NEB	Cat#C3040I
Chemicals, Peptides, and Recombinant Proteins		
Puromycin dihydrochloride from *Streptomyces alboniger*	Sigma-Aldrich	Cat#P7255-25MG
Harringtonine	Cayman Chemical Company	Cat#26833-85-2
MCP-HaloTag	Tim Stasevich, Morisaki et al., 2016	N/A
scFv(GCN4)-sfGFP-6xHis	This study	N/A
Janelia Fluor® 646	Janelia	Cat#1811539-59-9
Cy3 NHS Ester	Sigma-Aldrich	Cat#GE25-9004-72
Critical Commercial Assays		
Pierce Mouse IgG1 Fab and F(ab')2 Preparation Kit	ThermoFisher Scientific	Cat#44980
Alexa Fluor® 488 Protein Labeling Kit *3 labelings*	Invitrogen	Cat#A10235
Invitrogen Lipofectamine LTX Reagent with PLUS Reagent	ThermoFisher Scientific	Cat#15-338-100
Quikchange Lightning	Agilent Technologies	Cat#210518
Deposited Data		
raw data related to Figures 1 and 2	This study	https://doi.org/10.17632/wzyd4f55fp.1
raw data related to Figure 3	This study	https://doi.org/10.17632/h83tz96xyd.1
raw data related to Figure 4	This study	https://doi.org/10.17632/jvx5pm5yyk.1
raw data related to Figure 5	This study	https://doi.org/10.17632/bd9vccp26k.1
Model Codes	This study	https://Github.com/MunskyGroup/bursty_frameshift_source_code
Experimental Models: Cell Lines		
U-2 OS	ATCC	Cat#HTB-96
Oligonucleotides		
Frameshift sequence from HIV-1 RNA oligo (FSO)	IDTDNA, See Table S1	N/A
Scramble RNA Oligo (Scr)	IDTDNA, See Table S1	N/A
boxB stem-loop RNA oligo (BB)	IDTDNA, See Table S1	N/A
Forward primer, amplify XXLb1	IDTDNA, See Table S1	N/A
Reverse primer, amplify XXLb1	IDTDNA, See Table S1	N/A
Oligo inserted to replace FSS in control tag	IDTDNA, See Table S1	N/A
Oligo inserted to replace FSS in control tag and shift all frames +1 nucleotide	IDTDNA, See Table S1	N/A
Forward primer, amplify scFv(GCN4)-sfGFP	IDTDNA, See Table S1	N/A
Reverse primer, amplify scFv(GCN4)-sfGFP	IDTDNA, See Table S1	N/A
QuikChange Lightning oligo 1	IDTDNA, See Table S1	N/A
QuikChange Lightning oligo 2	IDTDNA, See Table S1	N/A

(*Continued on next page*)

Continued

REAGENT or RESOURCE	SOURCE	IDENTIFIER
Recombinant DNA		
+FSS multi-frame (MF) tag	This study, ThermoFisher Scientific GeneArt, See Table S1	N/A
+FSS reverse multi-frame (revMF) tag	This study, ThermoFisher Scientific GeneArt, See Table S1	N/A
pET21_scFv_sfGFP_GB1_6xHis	This study	N/A
pHR-scFv-GCN4-sfGFP-GB1-dWPRE, encoded HA epitope mutated	This study	N/A
smHA +FSS multi-frame (MF) tag	This study	N/A
-FSS control tag	This study	N/A
-FSS(+1nt) tag	This study	N/A
1XFLAG-revMF construct	This study	N/A
1XSunTag-MF construct	This study	N/A
Software and Algorithms		
Mathematica	Wolfram Research	N/A
Fiji	Schindelin et al., 2012	N/A
MATLAB	MathWorks	N/A

CONTACT FOR REAGENTS AND RESOURCE SHARING

Requests for further information and resources should be directed to and will be fulfilled by the corresponding authors, Brian Munsky (brian.munsky@colostate.edu) and Tim Stasevich (tim.stasevich@colostate.edu). Key plasmids will be deposited on Addgene.

METHOD DETAILS

Plasmid Construction

The HIV-1 frameshift sequence (FSS) followed by either the multi-frame (MF) tag or the reverse multi-frame (revMF) tag were synthesized by GeneArt® gene synthesis service (Thermo Fisher Scientific). The gene fragments were flanked by *NotI* and *NheI* and fused upstream of the beta-actin zipcode and 24x MS2 stem loops in the 3′ UTR of plasmid pUB_smFLAG_ActB_MS2 (Plasmid #81083, addgene) to obtain the FSS-MF and FSS-revMF, respectively. To double the MF tag, the MF tag region was digested out from FSS-MF with *XbaI* and *AgeI*, and then ligated into FSS-MF flanked with *NheI* and *AgeI*. The open reading frame encoding human XXLb1/AlexX (Abramowitz et al., 2004; Aydin et al., 2009) was amplified from U-2 OS cells cDNA with the primers: 5′- GTT GTC ATA TGG GCG TGC GCA ACT −3′; 5′- GAT GTA GCT AGC CTA GAA GCA GCA GGC GGT G −3′. The amplified XXLb1/AlexX was flanked with *NdeI* and *NheI*, and then inserted into the C-terminal region of the FSS-MF, FSS-2xMF and FSS-revMF to obtain FSS-MF-AlexX (i.e., the +FSS MF tag), FSS-2xMF-AlexX (i.e., the +FSS 2xMF tag), and FSS-revMF-AlexX (i.e., the +FSS revMF tag), respectively. To produce smHA-FSS-MF-AlexX (i.e., the HA MF tag), the spaghetti monster HA (smHA) (Viswanathan et al., 2015) was flanked with *NotI* and PstI, and then inserted into the N-terminal region of FSS-MF-AlexX. For the control constructs, FSS was removed using KpnI and *XbaI*. To keep the same frame for MF and AlexX, the following sequence was ligated between KpnI and *XbaI* to obtain MF-AlexX (i.e., the -FSS control tag): 5′- GGT ACC GGG AAT TTT CTT CAG AGC AGA CCA GAG CCA ACA GCC GCA CCG TTT CTA GA −3′. To shift the −1 frame into 0 frame for MF and AlexX, the following sequence was ligated between KpnI and *XbaI* to obtain MF-AlexX (the -FSS(+1nt) tag): 5′- CGG GAA TTT TCT TCA GAG CAG ACC AGA GCC AAC AGC CGC ACC GTT CT −3′.

scFv-sfGFP was amplified from pHR-scFv-GCN4-sfGFP-GB1-dWPRE (Plasmid #60907, addgene) using primers: 5′- GCG CGC ATA TGA TGG GCC CCG ACA TC −3′; 5′- GCC GGA ATT CGC CGC CTT CGG TTA CCG TGA AGG T −3′. The amplified scFv-sfGFP was flanked with NdeI and EcoRI, and then inserted into a pET21 vector backbone for expression and purification from *E.coli*.

For HA MF tag experiments, the HA epitope encoded in the scFv-sfGFP plasmid (Plasmid #60907) from Addgene was removed by site-directed mutagenesis with QuikChange Lightning (Agilent Technologies) per the manufacturer's instruction using primers: 5′- CCT CCG CCT CCA CCA GCG TAA TCT GAA CTA GCG GTT CTG CCG CTG CTC ACG GTC ACC AGG GTG CCC −3′; 5′- GGG CAC CCT GGT GAC CGT GAG CAG CGG CAG AAC CGC TAG TTC AGA TTA CGC TGG TGG AGG CGG AGG −3′.

Fab generation and dye-conjugation

Fab generation was done using the Pierce mouse IgG1 preparation kit (Thermo Fisher Scientific) per the manufacturer's instructions. Briefly, beads conjugated with ficin were incubated in 25 mM cysteine to digest FLAG (Wako, 012-22384 Anti DYKDDDDK mouse

IgG_{2b} monoclonal) or HA (Sigma-Aldrich, H3663 HA-7 IgG_1 mouse monoclonal) antibodies to generate Fab. Fab were separated from the digested Fc region using a NAb Protein A column (Thermo Scientific, product # 1860592). Fab were concentrated to ~1 mg/ml and conjugated to either Cy3 or Alexa Fluor 488 (A488). Cy3 N-hydroxysuccinimide ester (Invitrogen) or A488 tetrafluorophenyl ester (Invitrogen) was suspended in DMSO and stored at −20°C. 100 μg of Fab were mixed with 10 μL of 1M $NaHCO_3$, to a final volume of 100 μL. 2.66 μl of Cy3 (or 5 μL of A488) was added to this 100 μL mixture and incubated for 2 hours at room temperature with end-over-end rotation. The dye conjugated Fab were eluted from a PBS equilibrated PD-mini G-25 desalting column (GE Healthcare) to remove unconjugated dye. Dye conjugated Fabs then were concentrated in an Ultrafree 0.5 filter (10k-cut off; Millipore) to 1 mg/ml. This conjugation and concentration process was repeated on occasion to ensure a degree of labeling close to one. The ratio of Fab:dye, A_{rat}, was determined using the absorbance at 280 and 550 nm or 495 nm, the extinction coefficient of IgG at 280 nm, ε_{IgG}, the extinction coefficient of the dye, ε_{dye}, provided by the manufacturer, and the dye correction factor at 280 nm, *CF*, provided by the manufacturer. The degree of labeling, *DOL*, was calculated with the following formula:

$$DOL = \left(\frac{\varepsilon_{IgG}}{\varepsilon_{dye}}\right)\left(\frac{1}{(A_{rat})^{-1} - CF}\right). \quad (1)$$

Only Fab calculated with a *DOL* ~1 were used in experiments.

MCP and scFv-sfGFP purification

His-tagged MCP or scFv-sfGFP was purified over a Ni-NTA-agarose (QIAGEN) per the manufacturer's instructions with minor modifications. Briefly, bacteria were lysed in a PBS-based buffer with a complete set of protease inhibitors (Roche). Binding to the Ni-NTA resin was done in the presence of 10 mM imidazole. The resin was washed with 20 and 50 mM imidazole in PBS. The protein was then eluted in 300 mM imidazole in PBS. The eluted his-tagged MCP was dialyzed in a HEPES-based buffer (10% glycerol, 25 mM HEPES pH 7.9, 12.5 mM $MgCl_2$, 100 mM KCl, 0.1 mM EDTA, 0.01 % NP-40 detergent, and 1 mM DTT), snap-frozen in liquid nitrogen, and stored at −80C.

Cell culture, transfection, and bead-loading

U-2 OS cells were grown using DMEM (Thermo Scientific) supplemented with: 10% (v/v) FBS, 1 mM L-glutamine and 1% (v/v) Penicillin-streptomycin. Before experiments, cells were plated on a 35 mm MatTek chamber (MatTek) and DNA was either transiently transfected with Lipofectamine LTX (Thermo Scientific) per the manufacturer's instructions or transiently transfected via bead-loading. As described previously (Hayashi-Takanaka et al., 2011; Morisaki et al., 2016), bead-loading involved the following six steps: First, 100 μg/ml of fluorescently labeled Fab, 250 μg/ml of purified (GCN4) scFv-sfGFP and 33 μg/ml of purified MCP-HaloTag protein were mixed with PBS to a final volume of 4 μl. Second, in a cell culture hood, DMEM was aspirated from the MatTek chamber and the 4 μl mix was pipetted on top of cells. Third, ~106 μm glass beads (Sigma Aldrich) were evenly sprinkled over the cells. Fourth, the chamber was tapped carefully ~10 times on the cell culture hood bench top. Fifth, DMEM was immediately added back to the cells. Sixth, cells were returned to the incubator for at least an hour to recover from the loading procedure. In most experiments, we also bead-loaded DNA, which we added to the initial 4 μl mix (so that DNA had a final concentration close to 1 mg/ml). On occasion, DNA was transiently transfected ~2 hours before bead-loading. Around one hour before experiments began, bead-loaded cells were washed with phenol-red-free complete DMEM to remove glass beads, and 200 nM of JF646-HaloTag ligand (a cell permeable fluorogenic ligand (Grimm et al., 2015)) was added to label MCP-HaloTag protein. After 30 mins of incubation, cells were washed three times using phenol-red-free complete DMEM to remove any unconjugated fluorophores. Cells were then immediately imaged for experiments.

Single molecule tracking microscopy

To track single molecule translation sites, a custom-built widefield fluorescence microscope based on a highly inclined illumination scheme (Tokunaga et al., 2008) was used (Morisaki et al., 2016). Briefly, the excitation beams, 488, 561 and 637 nm solid-state lasers (Vortran), were coupled and focused at the back focal plane of the objective lens (60X, NA 1.49 oil immersion objective, Olympus). The emission signals were split by an imaging grade, ultra-flat dichroic mirror (T660lpxr, Chroma) and detected using two EM-CCD (iXon Ultra 888, Andor) cameras via focusing with 300 mm tube lenses (producing 100X images with 130 nm/pixel). With this setting, one camera detected far-red signals and the other detected either red or green signals. Far red signals were detected with the 637 nm laser and the 731/137 nm emission filter (FF01-731/137/25, Semrock). Red and green signals were separated by the combination of the excitation lasers and the emission filters installed in a filter wheel (HS-625 HSFW TTL, Finger Lakes Instrumentation); namely, the 561 nm laser and 593/46 nm emission filter (FF01-593/46-25, Semrock) were used for Cy3 imaging, and the 488 nm laser and 510/42 nm emission filter (FF01-510/42-25, Semrock) were used for sfGFP or A488 imaging. Live cells were placed into a stage top incubator set to a temperature of 37°C and supplemented with 5% CO_2 (Okolab) on a piezoelectric stage (PZU-2150, Applied Scientific Instrumentation). The focus was maintained using the CRISP Autofocus System (CRISP-890, Applied Scientific Instrumentation). The lasers, the cameras, the filter wheel, and the piezoelectric stage were synchronized via an Arduino Mega board (Arduino). Image acquisition was done with open source Micro-Manager software (Edelstein et al., 2014). Imaging size was set to 512 × 512 $pixels^2$ (66.6 × 66.6 μm^2), and exposure time was set to 53.64 msec. Readout time for the cameras from the combination of our imaging size,

readout mode, and the vertical shift speed was 23.36 msec, resulting in an imaging rate of 13 Hz (70 msec per image). The excitation laser lines were digitally synched to ensure they only illuminated cells when the camera was exposing in order to avoid excessive photobleaching. To capture the entire volume of the cytoplasm of U-2 OS cells, 13 z stacks with step size of 500 nm (6 μm in total) were imaged using the piezoelectric stage such that the z-position changed every 2 images (one image for Cy3 and one for sfGFP/A488 + JF646). The position of the filter wheel was changed during the camera readout time. This resulted in a total cellular imaging rate of 0.5 Hz (2 s per volume for 3-colors). Note that all colors described in the text and that are shown in the figures are based on the color of the excitation laser: RNA in red (JF646) and protein in green (Cy3) or blue (sfGFP/A488).

Particle tracking

Images were first pre-processed using either Fiji (Schindelin et al., 2012) or a custom-written batch processing *Mathematica* code (Wolfram Research) to make 2D maximum intensity projections from 3D images. Pre-processed images were then analyzed with a custom-written *Mathematica* code to detect and track particles. Specifically, particles were emphasized with a band-pass filter so the positions could be detected using the built-in Mathmatica routine ComponentMeasurements "IntensityCentroid." Detected particles were linked through time by allowing a maximum displacement of 5 pixels between consecutive frames. Particle tracks lasting at least 5-10 frames were selected and their precise coordinates were determined by fitting (using the built-in *Mathematica* routine NonlinearModelFit) the original 2D maximum intenstiy projected images to a 2D Gaussians of the following form:

$$I(x,y) = I_{BG} + Ie^{-\frac{(x-x_0)^2}{2\sigma_x^2} - \frac{(y-y_0)^2}{2\sigma_y^2}} \quad (2)$$

where I_{BG} is the background intensity, I the particle peak intensity, (σ_x, σ_y) the spread of the particle, and (x_0, y_0) the particle location. The offset between the two cameras was registered using the built-in *Mathematica* routine FindGeometricTransform to find the transform function that best aligned the fitted positions of 100 nm diameter Tetraspeck beads evenly spread out across the image field-of-view. We did not register the images, but only the fitted positions in order to avoid introducing any distortion into images. This is why a slight offset can be observed between the red and the green/blue particles even though they are within a diffraction limited spot, according to our registration.

For visuallization and some quantification, average intensity image trims were created by averaging images of all detected particles of a given species (each centered by their intensity centroid). To compute the average RNA signal intensity in a translation site (see Figure S3), the average image trims of RNA were fitted to Equation 2. The average intensities were calculated by integrating the fitted Gaussian. Fits were susceptible to noise, so we also used an alternative strategy to determine the average intensity of translation sites and RNA that was robust to noise (in all Figs aside from Figure S3). Specifically, the intensity of centered images of RNA or translation sites was calculated to be the average intensity within a centered radial spot of four pixels in diameter minus the average background intensity from a centered ring with an outer diameter of twelve pixels and an inner diameter of eight pixels. *Mathematica* source code is available upon request.

Calibrating translation site intensity

To calibrate the nascent chain intensity signals within translation sites to units of mature protein (i.e., to units that are roughly equivalent to the number of nascent chains or ribosomes within the translation site), two new calibration constructs were cloned. The calibration constructs are nearly identical in length and sequence to the original -FSS control construct (which lacks the frameshift sequence), but each harbors just a single epitope in the 0 frame: either a single FLAG epitope or a single SunTag epitope. In this way, each nascent chain in a translation site is labeled by just one fluorophore (from a single anti-FLAG Fab or a single anti-SunTag scFv). Thus, the intensity of a translation site will be equal to the number of nascent chains multiplied by the intensity of a single fluorophore. Because the intensity of a single fluorophore can be unambiguously measured via the observation of single step photobleaching, it is possible to estimate the number of nascent chains (or ribosomes) per translation site, i.e., convert the intensity signal into units of mature protein, as shown in Figures S2D–S2I.

To clone the calibration constructs, the FSS was removed from both the MF tag and the revMF tag using KpnI and *XbaI* digestion. Second, small oligos encoding a single SunTag epitope and single FLAG epitope were ligated between KpnI and *XbaI* of the MF tag and the revMF tag constructs, resulting in the 1XSunTag-MF and 1XFLAG-revMF constructs, respectively. The amplified XXLb1/AlexX was flanked with *NdeI* and *NheI* and then inserted into the C-terminal region of the 1XSunTag-MF and the 1XFLAG-revMF to obtain the 1XSunTag-MF-AlexX and 1XFLAG-revMF-AlexX calibration constructs. By design, these two constructs can be imaged in the same imaging session in separate dishes to directly compare 1X epitope (FLAG or SunTag) fluorescence to 12X epitope fluorescence in the MF or revMF tags (Figure S2D).

To calibrate translation site fluorescence intensity, cells transfected with the calibration constructs and bead-loaded with either anti-FLAG Fab (Cy3) or anti-SunTag scFv (sfGFP) were imaged in a single plane at high laser powers (50 mW for 561nm and 100mW for 488nm laser). A short movie was acquired, after which cells were continually imaged (without acquiring a movie) to photobleach them to the point at which single probe fluorescence could easily be detected by single-step photobleaching. At this point, a second short 250-frame movie was acquired. The intensity of polysomes (verified by the presence of an RNA signal intensity) from the the first frame of the first movie was then measured (as described in the 'Particle tracking' section above) and compared to the plateau intensity of a single probe just prior to single-step photobleaching. Examples of this procedure are shown in Figures S2E

and S2F. We performed calibration in this way to ensure at the beginning of the movie the epitopes would be close to saturation. Had we started from a lower concentration of probe (although this would enable single probe tracking without the need for photobleaching), the epitopes in polysomes would be less saturated, which would lead to an underestimate of the polysome fluorescence. From these measurements, the average number of nascent chains (or ribosomes) in a translation sites can be estimated from the intensity ratio of polysomes to single probes. Assuming the two calibration tags harbor the same number of ribosomes per translation site, their intensity ratios provide the conversion of the intensity of the MF tag or revMF tag to units of mature protein (see Figure S2D).

Translation Site Species Identification

After RNA particles were identified and tracked using the custom *Mathematica* code described above, an average centered image of the first five frames from each track was created for RNA (JF646), 0 ORF (FLAG-Cy3 in the +FSS MF tag), and −1 ORF (scFv-sfGFP in the +FSS MF tag). The trims were then hand checked to remove any trims with artifacts, e.g., smears or non-diffraction limited spots. Next, a custom *Mathematica* code was used to detect particles in the 0 ORF or −1 ORF trim channels, sorting the spots into RNA only, 0 frame translation sites (0 TS only), 0 and −1 TS, and −1 only TS. For all cases, RNA always had to be present. Finally, frameshifting translation sites (the 0 and −1 TS or the −1 only TS) were validated by eye, to further remove artifacts. For example, RNA that briefly colocalized with a mature protein punctae were removed at this stage. After all sites were validated, the total count of each type of species was used to determine the percentage of non-translating RNA (no TS), 0 frame translation sites (0 TS), 0 and −1 TS, and −1 only TS.

Puromycin treatment

To confirm active translation elongation, puromycin (Sigma Aldrich) was used to release nascent chains from elongating ribosomes, leading to a rapid loss of nascent chain signal at translation sites. Bead-loaded cells with visible translation sites were imaged at a rate of one volume every seven seconds. After acquiring 16 pre-images, cells were treated with a final concentration of 100 μg/ml puromycin and continuously imaged for an additional 100 time points. As a control, the same imaging conditions were performed except that the cells were treated with vehicle (H_2O). In this case, nascent chain signals did not disappear (data not shown). Both frameshifting and non-frameshifting translation sites were monitored through time using the tracking code described above.

Oligo RNA co-transfection

Uncapped RNA oligos containing the FSS from HIV-1 (FSO), a scrambled form of the FSO sequence (Scr), or the boxB stem-loop sequence (BB) were synthesized from IDTDNA with the following RNA sequences, respectively: 5′- UUU UUU AGG GAA GAU CUG GCC UUC CCA CAA GGG AAG GCC AG −3′, 5′- GAC GAA CUC AGG AUC GCC UUA GCG GAG UCU UAU UGA AUG GC −3′, or 5′- AUU CCU GGG CCC UGA AGA AGG GCC CCU CGA CUA AGU CCA AC −3′. Co-transfection of FSS-MF-AlexX and the RNA oligo was carried out via bead-loading, as described above. Briefly, 1 μg plasmid FSS-MF-AlexX construct DNA, 100 μg/ml of fluorescently labeled Fab, 250 μg/ml of purified (GCN4) scFv-sfGFP or 1 μg of (GCN4) scFv-sfGFP plasmid, 1 or 4 μg of RNA oligo, and 33 μg/ml of purified MCP-HaloTag protein were mixed with PBS to a final volume of ∼4 μl of PBS.

Ribosome Run-Off Experiments and fits

To measure the average elongation rate, harringtonine (Cayman Chemical) was used to block translation initiation and induce the run-off of all actively elongating ribosomes, leading to a gradual loss of nascent chain signal at translation sites. Bead-loaded cells with visible translation sites were imaged as described above except that cell volumes were acquired every 60 or 120 s. Laser powers were lowered (the 488 nm laser from 500 μW to 150 μW (3.3 times lower), the 561 nm laser from 900 μW to 500 μW (1.8 times lower), and the 647 nm laser from 1.5 mW to 1 mW (1.5 times lower)) to eliminate observable photobleaching of the green (Cy3 conjugated Fab) and blue (SunTag-scFv-sfGFP) channels. After acquiring 5 pre-images, cells were treated with a final concentration of 3 μg/ml Harringtonine and continuously imaged for 30 more time points. As a photobleaching control, cells with translation sites were imaged with the same image settings and number of frames, revealing no loss of nascent chain signal (data not shown). After experiments, the intensities of translation sites were measured as described above. The intensity of all translation sites in each frame (and in all cells) were then totaled to produce the run-off curve. Run-off curves were normalized to the mean of the total intensity of the first four time points after treatment of harringtonine began. These curves were then fit to a linear regression to roughly estimate run-off times (see Figure S4A). The linear portion of the run-off decay begins when the normalized run-off intensity reaches a fraction f_0:

$$f_0 = L1/(L1 + L2/2) \tag{3}$$

where $L1$ is the length of untagged portion of the open reading frame and $L2$ is the length of the tagged portion (i.e., the length of the repeated epitopes), as described (Morisaki and Stasevich, 2018). The linear portion of the decay was then interpolated to background levels to estimate the run-off time R_T. The elongation rate k_{el} was calculated as follows:

$$k_{el} = (L1 + L2/2)/R_T, \tag{4}$$

Fluorescence recovery after photobleaching (FRAP)

To confirm elongation rates of frameshifting translation sites, FRAP experiments were performed. Bead-loaded cells with visible translation sites were imaged once every 10 s, with an intentional photobleach at frame 10. The photobleach was performed with a 405 nm laser focused to a spot roughly 5 μm in diameter and operating at a minimal power such that the nascent chain signal did not completely vanish. This allowed us to track the translation site continously throughout the experiment. Following the intentional photobleach, the fluorescence recovery of translation sites within the bleach zone were monitored for an additional 80 time points. These translation sites were tracked and their intensities quantified, as described above. To correct for unintentional photobleaching, the loss of signal from the control translation site was fit to a single exponential decay and this decay was divided out from the FRAP recovery curves. The FRAP recovery curve can be thought of as the inverse of the harringtonine run-off curve (Morisaki and Stasevich, 2018). In this way, the FRAP recovery curve was fit to determine the average translation elongation rate (Figure S4B).

Statistical Analyses

For comparing cumulative distributions, we use the 2-sample KS test. For comparing mean values, we use the Mann Whitney U test. For fitted parameters, we use the fitted confidence intervals from *Mathematica's* built in NonlinearModelFit routine. In all figures, P values are displayed as: * $p < 0.05$; ** $p < 0.01$; *** $p < 0.001$; **** $p < 0.0001$.

General aspects of modeling frameshift kinetics

The frameshift models describe the stochastic dynamics of nascent translation with single-codon resolution. Both the constitutive and bursting models are formulated to track an arbitrary number of individual ribosomes that can perform three possible reactions: (i) A new ribosome can initiate translation at the start codon at rate k_{ini}. (ii) An existing ribosome can elongate at rate k_e to incorporate one amino acid into the nascent peptide chain. The rate k_e is sequence-specific with each codon's rate scaled by the genomic copy of the corresponding codon (Nakamura et al., 1999). When the ribosome completes the final amino acid, translation is terminated and that ribosome is eliminated. (iii) A ribosome at the frameshift sequence can shift from the 0 to the −1 frame. In addition to these three reactions, ribosomes at the frameshift sequence can pause for an average time of $1/k^*_{FSS}$ or $1/k_{FSS}$ for the shifted or non-shifted states. For the bursting model, each RNA is assumed to switch back and forth between non-frameshifting and frameshifting states with rates k_{on} and k_{off}. With these mechanisms and parameters, the models can be analyzed using either simplified approximations or detailed simulations.

Several approximate features can be derived directly from the bursting model parameters (see Table 1). The average burst time or time spent in a frameshifting state is:

$$\langle b^* \rangle = 1/k_{off}, \tag{5}$$

The average time spent in a non-frameshifting state is:

$$\langle b \rangle = 1/k_{on}. \tag{6}$$

The fraction of RNA in a frameshifting state is:

$$f^*_s = k_{on}/(k_{on} + k_{off}). \tag{7}$$

The number of ribosomes that initiate during the frameshifting state is:

$$r^*_i = k_{ini}/k_{off}. \tag{8}$$

The number of ribosomes that initiate during the non-frameshifting state is:

$$r_i = k_{ini}/k_{on}. \tag{9}$$

The time for a ribosome to clear the FSS in the frameshifting state is:

$$\tau^*_{FSS} = 1/k^*_{FSS} + \delta \cdot r_e/k_{el}, \tag{10}$$

where the second term accounts for ribosome pileup in the 9-codon ribosomal exclusion region (Ingolia et al., 2009), , upstream of the FSS. Similarly, the time for a ribosome to clear the FSS in the non-frameshifting state is:

$$\tau_{FSS} = 1/k_{FSS} + \delta \cdot r_e/k_{el}. \tag{11}$$

One can approximate $\delta = 1$ or 0 if initiation is faster $(k_{ini} > k_{FSS})$ or slower $(k_{FSS} > k_{ini})$ than the FSS pause.

The average elongation time for a ribosome in the frameshifting state is:

$$\langle \tau^*_e \rangle = gl/k_{el} + \tau^*_{FSS} \tag{12}$$

and the number to clear in a non-frameshifting state is:

$$\langle \tau_e \rangle = gl/k_{el} + \tau_{FSS}, \tag{13}$$

where gl is the gene length in codons.

Simulations were started at $t = -10{,}000$ s to approximate steady state at t = 0 using the Gillespie algorithm (Gillespie, 1976). Ribosome densities were found by collecting position statistics for multiple simulations. Simulated ribosome numbers and positions and multi-frame tag probe locations were combined to estimate translation site intensities. Harringtonine assays were simulated by preventing the initiation reaction at the time of treatment. Parameter estimation was performed using genetic algorithms and a multiple-objective cost function that considers the frameshifting efficiency, the number of ribosomes per RNA and the Harringtonine assays. A detailed description of the computational methods and codes is given in the 'Computational Details' section below.

Computational Details

Both the constitutive model and the bursting model consist of three general ribosomal reaction types: initiation (w_0), elongation (w_i or $\hat{w}_i$) and frameshifting (w_{FSS} or $\hat{w}_{FSS}$) as depicted in Equation 17,

$$\varnothing \xrightarrow{w_0} x_1 \xrightarrow{w_1} x_2 \xrightarrow{w_2} x_i \cdots \xrightarrow{w_i} x_{fs} \begin{cases} \xrightarrow{w_f} x_{i+1} \xrightarrow{w_{i+1}} x_{i+2} \xrightarrow{w_t} x_N \\ \xrightarrow{\hat{w}_f} y_1 \xrightarrow{\hat{w}_{i+1}} y_i \xrightarrow{\hat{w}_t} y_N \end{cases}, \tag{14}$$

Ribosome Initiation

Ribosomes are assumed to bind to the RNA with rate k_{ini}. To account for the fact that ribosomes are large biomolecules that occupy around 20 to 30 nuclear bases on the RNA (Ingolia et al., 2009), initiation is blocked by any downstream ribosome within $n_f = 9$ codons (in either frame). Therefore, the initiation rate is set at:

$$w_0 = \begin{cases} k_{ini}, & \text{if codons}\{1, \ldots, n_f\}\text{unoccupied}, \\ 0, & \text{otherwise}, \end{cases} \tag{15}$$

Ribosome Elongation

Each ribosome moves along the RNA codon by codon in the 5′ to 3′ direction. The elongation rate for each i^{th} codon, $\hat{k}_{el}$ is assumed to be:

$$w_i = \begin{cases} k_{el}(u_i/\overline{u}), & \text{if codons}\{i+1, \ldots, i+n_f\}\text{unoccupied}, \\ 0, & \text{otherwise}, \end{cases} \tag{16}$$

where u_i denotes the codon usage frequency in the human genome obtained from Nakamura et al. (1999), and $\overline{u}_i$ represents the average codon usage frequency in the human genome. The parameter k_{el}specifies the average elongation rate. Ribosomal termination is assumed to be equivalent to elongation of the final codon.

Frameshifting and Pausing

When the ribosome reaches the frameshift site, n_{FSS}, it pauses, and may shift from the 0 frame to the -1 frame. For the constitutive model, the ribosome can continue in the 0 frame with rate

$$w_{FSS} = \begin{cases} k_{FSS}, & \text{if codons}\{n_{FSS}+1, \ldots, n_{FSS}+n_f\}\text{unoccupied}, \\ 0, & \text{otherwise}, \end{cases} \tag{17}$$

or the ribosome can continue in the -1 frame at rate:

$$\hat{w}_{FSS} = \begin{cases} k^*_{FSS}, & \text{if codons}\{n_{FSS}+1, \ldots, n_{FSS}+n_f\}\text{unoccupied}, \\ 0, & \text{otherwise}, \end{cases} \tag{18}$$

For the bursting model, the decision to continue in the 0 or -1 frame depends upon the frameshifting state with the rate given by:

$$w_{FSS} \text{ or } \hat{w}_{FSS} = \begin{cases} k_{FSS}, & \text{if OFF and codons } \{n_{FSS}+1, \ldots, n_{FSS}+n_f\} \text{ unoccupied}, \\ k^*_{FSS}, & \text{if ON and codons}\{n_{FSS}+1, \ldots, n_{FSS}+n_f\}\text{unoccupied} \\ 0, & \text{otherwise}. \end{cases} \tag{19}$$

Relating model dynamics to experimental fluorescence intensity

To relate ribosome occupancy to experimental translation spots, we proscribe an assumed fluorescence to each ribosome based upon its position. This intensity is proportional to the number of epitopes upstream of the ribosome location and in the appropriate frame or frames. Ribosomes in the 0 frame include all upstream probes in the 0 frame. Ribosomes in the -1 frame include probes in

the 0 frame between the start codon and the FSS (if any) and probes in the −1 frame between the FSS and the current ribosome position. The total intensity vector for the j^{th} color is given by

$$I_j(t) = \sum_{i=1}^{N(t)} c_j(R_i(t)), \tag{20}$$

where $R_i(t)$ denotes the position (i.e., frame and codon location) of the i^{th} ribosome, $c_j(R_i)$ is the corresponding intensity of the j^{th} color, and $N(t)$ is the stochastically fluctuating number of translation ribosomes at time t.

Comparison of Data and Models

Fraction of translation spots. Experimental data was measured between 2 to 6 hours post bead-loading for a period of 120 s. To reproduce these experimental data, the model was solved using 2000 trajectories of 120 s starting at steady state. Spots were classified and their prevalence was reported as percentages for 0 frame only (P_{0F}), −1 frame only (P_{-1F}) and both frames (P_{BF}).

Intensities of translation sites per RNA

Nascent chain fluorescence in single translation sites was measured in units of mature protein (u.m.p.), as described in Figures S2D–S2I. Intensities were reported for translation spots containing −1 frame only (I_{-1F}), 0 frame only (I_{0F}), both frames in the green channel $(I_{BF/0})$ and both frames in the blue channel $(I_{BF/-1})$ (Figure 2 in the main text). In the bursting model, spots expressing both frames are those that have recently switched between 0 and −1 frame expression, but for which the ribosomes in the previous frame have not yet completed translation.

Ratio of intensities per RNA

To measure the average relative expression of frameshifted proteins, we calculated the ratio between the total intensity in the frameshifting and non-frameshifting translation spots, $R_{F:nFS}$, as follows:

$$R_{F:nFS} = \frac{\sum_{i=1}^{N} I_{-1F} + \sum_{i=1}^{N} I_{BF/-1}}{\sum_{i=1}^{N} I_{0F} + \sum_{i=1}^{N} I_{BF/0}}, \tag{21}$$

where $I_{(.)}$ denotes the steady-state intensity in each frame of the i^{th} translation spot. Under an assumption that the 0 frame and −1 frame proteins have equal degradation rates the production ratio $R_{F:nFS}$ would be expected to match the average steady-state ratio of mature protein in cells, which has previously been reported as 20:1 for the HIV Gag/Pol proteins (Brierley and Dos Ramos, 2006; Dulude et al., 2002; Grentzmann et al., 1998; Mouzakis et al., 2013).

Harringtonine assays

Harringtonine inhibits translation by binding to the ribosomal 60S sub-unit, which blocks new initiation events. Experimental data showed that harringtonine causes the intensity in translating spots to drop to a basal intensity value after a run-off time (Figure 4 in main text). To mimic the effects of harringtonine in our model, we modified the initiation rate as:

$$w_0 = \begin{cases} k_{ini}, & \text{if } t < t_H \text{ and codons}\{1, \ldots, n_f\}\text{unoccupied}, \\ 0, & \text{otherwise}, \end{cases} \tag{22}$$

where t_H is the time of application of harringtonine. After harringtonine application, spots simulated from the original construct were classified as 0 frame only (0F) or both 0 frame and −1 frames (BF). After classification, average spot intensities were quantified as:

$$H_{0F}(t) = I_{0F}(t) + b_{0F}, \tag{23}$$

$$H_{BF}(t) = I_{BF}(t) + b_{BF}, \tag{24}$$

where $b_{(.)}$ is experimental background expression obtained at the end of the experimental time of the run-off assays. Similarly, spots simulated for the extended construct with upstream HA tags and downstream −1 tags were classified as HA in non-shifted spots (HA) or HA in shifted spots (HA*).

$$H_{HA}(t) = I_{HA}(t) + b_{HA}, \tag{25}$$

$$H_{HA^*}(t) = I_{HA^*}(t) + b_{HA^*}. \tag{26}$$

Parameter estimation

For each model, we sought to find a single parameter set that reproduces all experimental data. Given the diversity of sources and types of experimental data, we estimated the parameter values using a multi-objective optimization strategy to simultaneously compare the fractions of shifted, non-shifted, and transiently shifting spots, the spot intensities for both frames, ratio of spot intensities and the Harringtonine run-off data, as follows:

$$J(\theta) = w_P \sum_{f=1}^{F} \left| \log_{10}\left(\widehat{P}_f(\theta) \Big/ \tilde{P}_f\right) \right| + w_I \sum_{f=1}^{F} \left| \tilde{I}_f - \widehat{I}_f(\theta) \right| + w_R \sum_{f=1}^{F} \left| \tilde{R}_{F:nFS,f} - \widehat{R}_{F:nFS,f}(\theta) \right| + w_H \sum_{c=1}^{C} \sum_{f=1}^{F} \sqrt{\frac{\sum_{t=1}^{T} \left(\tilde{H}_{t,f,c} - \widehat{H}_{t,f,c}(\theta)\right)^2}{T}}, \quad (27)$$

where experimental data are denoted as $\tilde{x}$ and simulations results as $\widehat{x}$. Weights (w_P, w_I, w_R and w_H) were used to balance constraints by the different experiments and time points. T represents the number of experimental points in the harringtonine assays, F is the number of studied frames, C is the number of different gene constructs. The first term in the objective function constrains the model to fit approximately to the 0 only, −1 only, and both frame fractions of translating spots and was expressed in terms of the sum of absolute log10 differences (i.e., fold changes rather than absolute differences) between the model and data, with weight $w_P = 1$. The weight used on the Harringtonine dataset was defined as $w_H = 1/(C \cdot F)$. The weight used to compare the ratio of intensities was defined as $w_R = 1/\tilde{R}_f$. The weight used to compare intensities was defined as: $w_I = \sum_{f=1}^{F} \tilde{I}_f$.

Parameter searches

Parameter searches consisted of optimization routines based on the pattern search algorithm. Pattern search optimization is an iterative approach that directs the search of parameters by evaluating the effects of varying one parameter at a time in the objective function. The size of the variation and direction of the search are directed by the changes in the objective function (Hooke and Jeeves, 1961).

The constitutive model has a total of four fitting parameters (k_{el}, k_{ini}, k_{FSS} and k^*_{FSS}). Although the bursting model has two additional parameters (k_{on}, k_{off}), the parameter k_{off} was directly determined from data in Figure 5B, and parameter k_{on} was included in the optimization routine, leading to five parameters total for that model. The parameter set that best reproduces the data was selected as:

$$\theta_{fit} = \underset{\theta}{\operatorname{argmin}} J(\theta). \quad (28)$$

Optimized parameter values are given in full detail in Table 1 for the bursting model.

Simulation details

To simulate the model's stochastic dynamics, we used the direct method from Gillespie's algorithm (Gillespie, 1976) coded in MATLAB. The pattern search algorithm was used for parameter optimization (Hooke and Jeeves, 1961). Parameter uncertainty analyses for the bursty model were calculated by building parameter distributions that reproduce results within a 10% error, calculated from 10,000 independent simulations using randomly selected parameter values. Simulations were performed on the W. M. Keck High Performance Computing Cluster at Colorado State University.

DATA AND SOFTWARE AVAILABILITY

The accession number for the Figures 1 & 2 data reported in this paper is Mendeley: https://doi.org/10.17632/wzyd4f55fp.1. The accession number for the Figure 3 data reported in this paper is Mendeley: https://doi.org/10.17632/h83tz96xyd.1. The accession number for the Figure 4 data reported in this paper is Mendeley: https://doi.org/10.17632/jvx5pm5yyk.1. The accession number for the Figure 5 data reported in this paper is Mendeley: https://doi.org/10.17632/bd9vccp26k.1. The accession number for the model code reported in this paper is Github: https://Github.com/MunskyGroup/bursty_frameshift_source_code.